

AMERICAN UNIVERSITY OF BEIRUT

EFFECT OF THERMAL CREEP ON THE BEHAVIOR OF FLUSH
ENDPLATE CONNECTIONS DUE TO FIRE TEMPERATURES

by
AHMAD HOUSNI EL GHOR

A thesis
submitted in partial fulfillment of the requirements
for the degree of Master of Engineering
to the Department of Civil and Environmental Engineering
of the Faculty of Engineering and Architecture
at the American University of Beirut

Beirut, Lebanon
January 2017

AMERICAN UNIVERSITY OF BEIRUT

EFFECT OF THERMAL CREEP ON THE BEHAVIOR OF FLUSH
ENDPLATE CONNECTIONS DUE TO FIRE TEMPERATURES

by
AHMAD HOUSNI EL GHOR

Approved by:



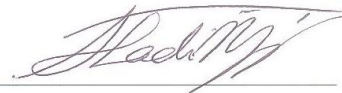
Dr. Elie G. Hantouche, Assistant Professor
Department of Civil and Environmental Engineering

Advisor



Dr. George Saad, Assistant Professor
Department of Civil and Environmental Engineering

Committee Member



Dr. Shadi Najjar, Associate Professor
Department of Civil and Environmental Engineering

Committee Member

Date of thesis defense: January, 27, 2017

AMERICAN UNIVERSITY OF BEIRUT

THESIS, DISSERTATION, PROJECT RELEASE FORM

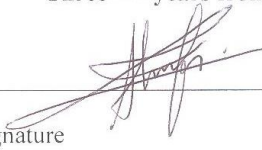
Student Name: EL Ghor Ahmad Housni
Last First Middle

Master's Thesis Master's Project Doctoral Dissertation

I authorize the American University of Beirut to: (a) reproduce hard or electronic copies of my thesis, dissertation, or project; (b) include such copies in the archives and digital repositories of the University; and (c) make freely available such copies to third parties for research or educational purposes.

I authorize the American University of Beirut, to: (a) reproduce hard or electronic copies of it; (b) include such copies in the archives and digital repositories of the University; and (c) make freely available such copies to third parties for research or educational purposes after:

- One ~~---~~ [✓] year from the date of submission of my thesis, dissertation, or project.
- Two ---- years from the date of submission of my thesis, dissertation, or project.
- Three ---- years from the date of submission of my thesis, dissertation, or project.


Signature

Feb. 7 2017
Date

ACKNOWLEDGMENTS

I do not believe any expression of gratitude is fit enough to describe my appreciation for all the support, patience, guidance, education, and all time I was granted from my advisor Dr. Elie G. Hantouche. His expertise and dedication were essential in the successful development of this research work. I appreciate his constant support and valuable critics which helped me develop my research skills, and knowledge throughout the time spent at the American University of Beirut.

I would also like to thank Dr. Mohamad Ali Morovat, Research Scientist Associate at the University of Texas at Austin, for his valuable efforts, time, and helpful discussions throughout the research.

My recognition and gratitude are also extended to my committee Dr. George Saad and Dr. Shadi Najjar.

Furthermore, I would like to gratefully acknowledge the financial support provided by the American University of Beirut Research Board under grant No.21113-102726, and by the Lebanese National Council for Scientific Research (LNCSR) under grant No. 103091-22968. Least but not last, I would like to thank researchers at the University of Sheffield for making the connection test results publicly available.

Finally, I would like to express gratitude to my family, friends, and my professor at Beirut Arab University Dr. Adnan Masri, for their support in the pursuit of my degree.

AN ABSTRACT OF THE THESIS OF

Ahmad Housni El Ghor for Master of Engineering
Major: Civil and Environmental Engineering

Title: Effect of Thermal Creep on the Behavior of Flush Endplate Connections Due to Fire Temperatures

The objective of this study is to investigate the effect of thermal creep of steel on the behavior of flush endplate beam-column connections subjected to elevated temperatures. Creep refers to the time-dependent inelastic deformation of structural steel at high temperatures. To address this issue, finite element (FE) models using ABAQUS are first developed to reproduce the experimental results available in the literature and specifically the total force-connection rotation characteristics of the connection under combined shear and tension forces during fire without creep effect. Then, a series of FE models for the same connection are developed to investigate the effect of creep on the behavior of flush end plate connections at different elevated temperatures with different load ratios. Different geometrical parameters are incorporated in this study such as load angle, plate thickness, and bolt diameter to investigate their effects on the overall thermal creep response of flush endplate connections in fire. In this methodology, time effects on the strength of flush endplate connections are explicitly considered in the form of isochronous force-rotation curves. This will help developing a holistic performance-based methodology to evaluate the performance of steel connections in fire.

Using experimental results available in the literature and finite element (FE) models conducted in ABAQUS, a mechanical model is developed to predict the total force-connection rotation characteristics of flush endplate connections at elevated temperatures including creep effect. The proposed model consists of multi-linear springs that predict each component stiffness, strength, and rotation. The multi-linear springs temperature expressions are based on the ambient temperature formulations proposed in *Eurocode3 Part 1.8* where material properties are considered temperature dependent. To include the effect of creep, modified *Burgers* creep model is used to predict the time-dependent connection rotation and temperature of the flush endplate connections. The modified *Burgers* creep model consists of linear springs and viscous dashpots that predict time-dependent connection rotation. The proposed model is validated against experimental results available in the literature and finite element (FE) models developed as a part of this study.

Through explicit consideration of thermal creep structural steel, the proposed model helps providing important insights into fire-induced thermal stresses and deformation and their implications on designing of flush endplate connections in fire.

CONTENTS

ACKNOWLEDGEMENTS	v
ABSTRACT.....	vi
LIST OF ILLUSTRATIONS.....	x
LIST OF TABLES.....	xiii
LIST OF ABBREVIATIONS.....	xiv

Chapter

1. INTRODUCTION.....	1
2. THERMAL CREEP OF STRUCTURAL STEEL	7
A. Creep Phenomenon.....	7
B. Creep of ASTM A36 steel at elevated temperatures	7
3. THERMAL CREEP BEHAVIOR OF FLUSH ENDPLATE CONNECTIONS IN FIRE	9
A. Development of the FE modeling	9
1. Flush endplate connection prototype	9
2. Boundary conditions	9
3. Material properties and modeling considerations	10
4. Model discretization.....	10
B. Development of methodology	11
C. Application of methodology	13
4. PARAMETERS AFFECTING THE TIME-DEPENDENT BEHAVIOR	29
A. Parameters affecting the time-dependent behavior of flush endplate connections in fire	29

1. Load angle.....	29
2. Endplate thickness	30
3. Bolt diameter.....	30
4. M27 bolt with 8 mm endplate thickness.....	31
5. MECHANICAL MODELING.....	40
A. Component stiffness	40
1. Column web in tension	40
2. Column web in compression.....	41
3. Column web panel in shear.....	41
4. Column flange in bending.....	42
5. Endplate in bending	42
6. Tension bolts.....	42
B. Equivalent connection stiffness	43
C. Determination of rotational stiffness	44
D. Moment and force-rotation curve for flush endplate connection	44
E. Connection resistance	46
1. Moment resistance, $M_{j,Rd}$:	46
2. Column flange in bending, $F_{t,cf,Rd}$:	47
3. Column web in tension, $F_{t,cw,Rd}$:	47
4. Endplate in bending, $F_{t,ep,Rd}$:	47
5. Beam web in tension, $F_{t,bw,Rd}$:	48
6. The maximum bending moment of the connection, M_{cd} :	48
F. Inclusion of thermal creep in the mechanical model.....	48
1. Modified Burgers model.....	49
2. Maximum connection rotation prediction.....	52
3. Effect of different geometrical parameters on the time-dependent behavior of flush endplate connections in fire	53
G. Proposed model performance	53
6. SUMMARY, CONCLUSIONS AND, RECOMMENDATIONS	65
A. Summary and conclusions.....	65
B. Recommendations	67

BIBLIOGRAPHY68

ILLUSTRATIONS

Figure		Page
1.	Qualitative representation of creep curve for structural steel.	8
2.	Flush endplate connection configuration used in simulations in ABAQUS.	16
3.	Flush endplate connection configuration utilized in the study.	17
4.	Time-independent strength of flush endplate connections at ambient and elevated temperatures.	17
5.	Time-independent connection deformation of flush endplate connections at 20°C.	18
6.	Time-independent endplate deformation of flush endplate connections at 450°C.	18
7.	Thermal creep behavior of flush endplate connection at 450 °C: (a) Total tensile stress in top bolts vs. time, (b) Connection rotation vs. time.	19
8.	Thermal creep behavior of flush endplate connection at 475 °C: (a) Total tensile stress in top bolts vs. time, (b) Connection rotation vs. time.	20
9.	Thermal creep behavior of flush endplate connection at 500 °C: (a) Total tensile stress in top bolts vs. time, (b) Connection rotation vs. time.	21
10.	Thermal creep behavior of flush endplate connection at 525 °C: (a) Total tensile stress in top bolts vs. time, (b) Connection rotation vs. time.	22
11.	Thermal creep behavior of flush endplate connection at 550 °C: (a) Total tensile stress in top bolts vs. time, (b) Connection rotation vs. time.	23
12.	Thermal creep behavior of flush endplate connection at 575 °C: (a) Total tensile stress in top bolts vs. time, (b) Connection rotation vs. time.	24
13.	Thermal creep behavior of flush endplate connection at 600 °C: (a) Total tensile stress in top bolts vs. time, (b) Connection rotation vs. time.	25
14.	Isochronous force-rotation curves for the flush endplate connection in consideration at 550 °C.	26
15.	Isochronous rotation-temperature curves corresponding to the constant load of 76 kN.	26
16.	3D Representation of isochronous rotation-temperature curves corresponding to the constant load of 76 kN.	27

17.	Isochronous rotation-temperature curves under variable loads.	28
18.	Effect of Load angle on the time-dependent behavior of flush endplate connection at: (a) 475 °C, (b) 550 °C, (c) 600 °C.	33
19.	Effect of endplate thickness on the time-dependent behavior of flush endplate connection at: (a) 475°C, (b) 550 °C, (c) 600 °C.	35
20.	Creep behavior of flush endplate connection with M27 bolts at 550 °C: (a) Total tensile stress in top bolts vs. time, (b) Connection rotation vs. time.	36
21.	Creep behavior of flush endplate connection with M27 bolts at 600 °C: (a) Total tensile stress in top bolts vs. time, (b) Connection rotation vs. time.	37
22.	Stress relaxation in the endplates of test conducted at: (a) 500 °C, (b) 600 °C	38
23.	Creep behavior of flush endplate connection with M27 bolts and 8 mm endplate thickness at 500 °C: (a) Total tensile stress in top bolts vs. time, (b) Connection rotation vs. time.	39
24.	Flush endplate connection configuration utilized in the study: (a) geometrical properties,(b) component stiffnesses assembly including dashpots.	56
25.	Tri-linear moment-rotation characteristic.	57
26.	Modified <i>Burgers</i> model.	57
27.	Time-dependent connection behavior: (a) Maxwell dashpot, (b) <i>Kelvin-Voight</i> model, (c) Modified <i>Burgers</i> model.	58
28.	Time-independent behavior of flush endplate connection: (a) Experimental vs. FE vs. mechanical model predictions, (b) FE vs. mechanical model predictions.	59
29.	FE vs. mechanical model of flush endplate connection behavior at: (a) 450 °C, (b) 475 °C, (c) 500 °C, (d) 525 °C.	61
30.	FE vs. mechanical model of flush endplate connection behavior at: (a) 550 °C, (b) 575 °C, (c) 600 °C.	63
31.	Iscochronous temperature-rotation curves: FE vs.mechanical model time-dependent connection rotation predictions	63

32. FE vs. mechanical model of flush endplate connection behavior at: (a) 500 °C with M27 bolts, (b) 500 °C with M27 bolts and 8 mm endplate, (c) 550 °C with 8 mm endplate. 65

TABLES

Table		Page
1.	Ultimate loads predicted from steady-state temperature analysis at different elevated temperatures	15
2.	Constants used in modified <i>Burgers</i> model equation.....	55
3.	Constants used in estimating the maximum connection rotation.....	56

LIST OF ABBREVIATIONS

A_b : effective area of the tension bolts

A_c : cross section area of the column

A_{vc} : shear area of column web

a_p : effective weld thickness

a, b , and c : constants available in table 3

b_c : width of column section

$b_{eff,cw,t}$: effective width of column web in tension

$b_{eff,cw,c}$: effective width of column web in compression

$b_{eff,t,wb}$: effective length of the equivalent T-stub representing the endplate in bending

c_1, c_2, c_3, c_4, c_5 , and c_6 : constants tabulated in table 2

d_b : bolt diameter

d_{cw} : clear depth of column web

d_{M20} : M20 bolt diameter

E : modulus of elasticity of the component

e : distance between the bolt centerline and the upper edge of the column flange

$F_{b,max}$: maximum load applied on the top bolts due to combined shear and tension forces applied
on the connection

$F_{tr,Rd}$: effective design tension resistance of bolt row n

$F_{t,cf,Rd}$: tension resistance of column flange in bending

$F_{t,ep,Rd}$: tension resistance of endplate in bending

$F_{t,cw,Rd}$: design resistance of an unstiffened column web subject to transverse tension

$F_{t,bw,Rd}$: tension resistance of beam web in tension

f_{nt} : nominal tensile strength of the bolt

f_{nv} : nominal shear strength of the bolt

f_v : required shear stress due to applied load

$f_{yt,cf}$: yield strength of the column flange at given temperature

$f_{yt,cw}$: yield strength of the column web at given temperature

$f_{yt,ep}$: yield strength of the endplate at given temperature

$f_{yt,wb}$: yield strength of the beam web at given temperature

$\frac{f_{ut,b}}{f_{yt,b}}$: ratio used to estimate the maximum moment for top bolts failure

$\frac{f_{ut,ep}}{f_{yt,ep}}$: ratio used to estimate the maximum moment endplate failure

$\frac{f_{y,b}}{f_{u,b}}$: ratio used to account for strain hardening of the bolt material

$\left(\frac{f_{yT}}{f_{uT}}\right)_F$: yield strength to tensile strength ratio for the connection component that governs the behavior of the connection

h_n : lever arm that can be taken from the center of rotation to the center-line of the bolt row n acting in tension

I_b : the moment of inertia for the bolt group

l_a : applied load

$K_{cw,t}$: column web stiffness in tension

$K_{cf,b}$: flexural stiffness of the column flange

$K_{ep,b}$: flexural stiffness of the end plate

K_{bt} : tension bolt stiffness

$K_{cwp,s}$: column web panel in shear stiffness

$K_{cw,c}$: column web stiffness

K_{eq} : equivalent spring stiffness

$K_{t,n}$: equivalent tension zone spring stiffness for a single bolt row at a given temperature

K_1 : linear spring used in *Maxwell* model

K_2 : linear spring used in *Kelvin-Voight* model

L_b : bolt elongation length

$l_{eff,cf,b}$: effective length of column flange in tension

$l_{eff,ep,b}$: effective length for endplate in tension

$M_{j,Ed}$: the applied bending moment

$M_{j,Rd}$: design moment connection resistance

$M_{pl,fc}$: plastic moment capacity of an equivalent T-stub

$M_{pl,ep}$: plastic moment capacity of an equivalent T-stub

M_{Cd} : maximum applied moment at failure of the connection

m : clear distance between the angle fillet and the bolt centerline

n : bolt-row number

P : peak load that the connection can withstand at any temperature

r : total connection rotation

r_1 : time-dependent rotation resulted from dashpot η_1

r_2 : time-dependent connection rotation resulted from the *Kelvin-Voight* model

\dot{r}_2 : connection rotation rate resulted from the *Kelvin-Voight* model

r_M : total rotation of *Maxwell* model

S_j : rotational stiffness

$S_{j,ini}$: initial rotational stiffness of the connection

s : equal to the root radius (r_c) for a rolled I or H section column

s_p : length obtained by dispersion at 45° through the end-plate

T : temperature in ($^\circ\text{C}$)

t : time

t_{10} : 10 mm plate thickness

t_{cw} : thickness of column web

t_{fb} : beam flange thickness

t_{ep} : endplate thickness

t_{cf} : column flange thickness

t_{wb} : the thickness of the beam web

x : the distance from the bottom of the endplate to the neutral axis of the bolt group

y_n : the distance from the bottom of the endplate to the center-line of each bolt row

Z_{eq} : equivalent lever arm

z : lever arm and is assumed to be taken as Z_{eq}

z' : lever arm which is approximately equal to the distance between the center of the lower beam flange to the midway between the farthest two bolt rows

α : bolt diameter dimensionless factor

γ : plate thickness dimensionless factor

β : transformation parameter that is approximately equal to 1 for one sided beam-column joint

μ : stiffness ratio

λ : stiffness modification coefficient

ω : reduction factor to allow for the interaction with shear in the column web panel

γ_{Mo} : partial factor for resistance of cross section and is equal to 1 for buildings

η_1 : viscous dashpot used in *Maxwell* model

η_2 : viscous dashpot used in *Kelvin-Voight* model

σ_0 : constant stress

θ_{Id} : connection rotation at which $M_{j,Ed}$ reaches $M_{j,Rd}$

θ_{Xd} : the connection rotation at which $M_{j,Ed}$ reaches $M_{j,Rd}$

θ_{Cd} : maximum rotation capacity that the connection can undergo

θ : time-independent connection rotation

$\theta_{(%P)}^t$: maximum time-dependent connection rotation that the connection can withstand

$\theta_{(%P)_{Total}}$: maximum connection rotation that the connection can withstand including thermal creep effect at any load to peak load ratio

θ_p : the maximum connection rotation that the connection can resist under steady-state temperature analysis

$\theta_{\%P}$: the connection rotation that the connection can undergo at any load to peak load ratio excluding thermal creep effect

CHAPTER I

INTRODUCTION

Performance-based design for structural fire safety allows engineers to predict the thermal and structural behavior of steel buildings in fire situations. These predictions help evaluating the induced moment capacities that connections can withstand at elevated temperatures. Flush endplate connections are one of the extensively used moment-resistant connections in steel buildings due to ease of construction and fabrication. At ambient temperature, flush endplate connections allow energy dissipation and provide a good response under both gravity and seismic loading. However, during a fire, different components of the flush endplate connections can undergo significant loss of strength and stiffness. Large axial forces are also developed in these connections and the connecting beams as a result of restraints to thermal displacements (Yu et al. 2011). Moreover, steel flush endplate connections in fire are subjected to significant rotation demands. These large deformation and force demands combined with loss of strength can potentially result in the failure of flush endplate connections during and after a fire (Al-Jabri et al. 2008; Yu et al. 2011; Li et al. 2012; and Geo et al. 2013). Failure of flush endplate connections due to fire does not depend only on loading capacity and temperature but also on the time duration of the applied load. Furthermore, one of the critical factors affecting the connection behavior at elevated temperature is the influence of creep material.

Many experimental and analytical studies were conducted in the past few years to investigate the behavior of flush endplate connections subjected to fire. Experimental tests and numerical analysis were conducted to investigate the behavior of flush endplate connections at elevated temperatures (Yu et al. 2011). Different parameters affecting the behavior of the connection such as load angle, bolt row, and endplate thickness were incorporated in the tests. The

results showed that endplate failure occurred at low temperatures (20 °C and 450 °C) whereas bolt failure occurred at high temperatures (550 °C and 650 °C). Also, three experimental tests were carried out to study the fire resistance capacity of flush endplate bolted composite connection in fire (Li et al. 2012). The results showed that significant local buckling of the bottom flange occurred in a test where the beam is not axially restrained (*test1*), while large axial compressive forces developed in the restrained beam (*tests 2 and 3*) and then changed to large tensile force at larger deflection. Furthermore, six experimental tests were performed to investigate the resistance of flush endplate connections under combined shear and tension during a fire (Geo et al. 2013). Two different endplate thicknesses of 8 mm and 16 mm were used in this study. The FE and the experimental results showed that in all cases the ultimate fracture was due to bolts failure, and severe bending deformation of the 8 mm endplate was significant. Besides, the study showed that the increase of either the shear or tension force will reduce the failure temperature of the connection, and stiffer endplates can increase the shear resistance of the connection under fire. Another numerical investigation was conducted using ABAQUS to establish the moment-rotation characteristics of the flush endplate connection under elevated temperatures (Al-Jabri et al. 2008). The results showed that the FE simulations predicted with good agreement the experimental failure modes and moment-rotation-temperature characteristics of the connection. In addition to that, a numerical investigation was conducted to study the behavior of a double angle connection under heating and cooling phases of a fire (Hantouche et al. 2016). Different parameters were included in this study such as load ratio, initial cooling temperature, double angle location, and gap distance. In addition, a detailed comparison was developed between the performance of double angle and shear tab connections when subjected to fire. The results show that the double angle connection is quite robust for fire loading and it has better performance at elevated temperature when compared

to shear tab connection. Also, another investigation was conducted to compare the response of double angle and shear endplate connections at elevated temperature (Hantouche and Sleiman 2016). The results show that beam bearing failure and plate rupture at the toe of the weld controlled the behavior of double angle and shear endplate connections, respectively. Also, the capacity of the double angle is greater than that of the shear endplate connection at ambient and elevated temperatures

Mechanical or stiffness modeling or known in the Eurocode3 part 1.8 (Eurocode3 2005) as component based modeling is considered as a rational model that requires the minimum computational effort while retaining the key behavioral characteristics of the connection and offering acceptable predictions of the overall response of bare steel connections at ambient and elevated temperatures. Previous mechanical models were developed for flush endplate connection to predict its time-independent behavior at elevated temperatures specifically the moment-connection rotation characteristics (Leston-Jones 1997; De Silva 2001; Block 2007; and Huang 2011). Also, the effect of thermal axial force was incorporated in the previous studies to examine its influence on the response of shear and flush endplate connections (Al Jabri 2004; Huang 2011; Hantouche and Sleiman 2016). All previous studies did not take into account the effect of time-dependent creep material, and neglecting creep effect may results in an unsafe design of beam-column steel connections subjected to fire.

The stress-strain behavior of structural steel at elevated temperatures has been shown to be highly time-dependent for some ranges of stresses and temperatures expected during a building fire (Morovat el al. 2011 and Morovat el al. 2012). Very limited research work has been conducted so far for modeling the effect of creep on structural steel elements. A numerical investigation (Kodur and Dwaikat 2010) was conducted using ANSYS and validated against experimental test

data (Li and Guo 2008) to study the effect of high temperature creep on the fire response of restrained steel beams. ANSYS creep model and Harmathy (Harmathy 1967) creep model were incorporated to account for the effect of high temperature creep on restrained beams. Then, a series of parametric studies were conducted to investigate the effect of load level, heating rate, fire scenario and degree of induced axial restraint on the extent of creep deformations. Results showed that Harmathy creep model (Harmathy 1967) is sufficient for predicting the creep deformation for unprotected steel members, but becomes inaccurate when high stress and temperature are maintained in steel members for a long time duration. Also, neglecting high temperature creep in fire resistance analysis might lead to unconservative fire resistance predictions in restrained beams. Another investigation (Li and Zhang 2012) was performed to examine the creep effect of axially restrained steel columns in real fire. Experimental models were validated and used to investigate the effect of load ratio, axial restraint ratio, and different fire scenarios on column buckling behavior. The creep effect was modeled using a combination between *Lie* model (Lie and Macaulay 1989) and ANSYS implicit creep model. The results show that for axially restrained steel columns in slow fire rates, creep will induce higher buckling temperatures when compared to models without including creep effect. While in case of fast fire rates, creep might give higher or lower buckling temperatures. Also, another examination (Morovat et al. 2011) was done to study the effect of creep on the buckling strength of steel columns using Harmathy (Harmathy 1967) and Fields and Fields (Fields and Fields 1989) creep models. It was shown that the buckling load strength of steel column depends not only on the applied load and temperature but also on the time duration for which the load was applied, and neglecting creep effect can lead to unsafe predictions of the strength of steel columns subjected to fire. Further, a recent numerical investigation (El Ghor et al. 2016) was conducted using ABAQUS to examine the time-dependent

nature of flush endplate connections in fire. Fields and Fields (Fields and Fields 1989) creep models was included in this analysis to take into account creep material in the beam and endplate. The results show that the creep behavior of flush endplate connections are highly time-dependent for temperatures above 500 °C and neglecting creep can result in unsafe predictions of the overall response of flush endplate connections subjected to fire. In addition, a very recent research developed a rheological (mechanical) model to predict the behavior of A36 steel at high temperature under stress and strain rate controlled test (Torić and Burgess 2016). The rheological model consisted of two “Kelvin-Voigt elements” and was able to model creep strain development under steady-state and transient heating conditions. All these studies did not develop a mechanical model to predict the time-dependent response of flush endplate connections subjected to elevated temperatures due to fire.

In an effort to address this shortcoming, this research proposes a typical methodology and a mechanical model to characterize the time-independent and time-dependent strength and deformation capacity of flush endplate connections when subjected to fire. First, FE simulations of flush endplate connections are conducted in ABAQUS under steady-state temperature analysis to reproduce the experimental work available in the literature (University of Sheffield 2007). Second, a series of FE simulations is conducted in ABAQUS on the same connection to study the effect of thermal creep behavior on flush endplate connection under steady-state creep analysis. Different geometrical parameters are incorporated in this study such as load angle, plate thicknesses, and bolt diameter to investigate their effects on the overall creep response of flush endplate connection in fire. Also, different load to peak load ratios were applied on the connection at different elevated temperatures to study the thermal creep behavior of flush endplate connection when both temperature and load are kept constant. This will help to develop a transient thermal

creep analysis to evaluate the creep effect on the performance of flush endplate connections in a real fire. This aims in providing a set of data to develop a mechanical model to account for the thermally-induced stresses and deformations and their implications on the design of flush endplate connections under fire loading taking into account the effect of thermal creep material.

CHAPTER II

THERMAL CREEP OF STRUCTURAL STEEL

A. Creep Phenomenon

Creep is defined as the time-dependent plastic strain under constant stress and temperature conditions. It is often stated that steel creep occurs when the temperature of steel exceeds one-third to half of the steel melting temperature. The creep of steel is a complex phenomenon that depends on steel material type, applied stress, temperature, time duration, and stress and temperature histories. It includes the phenomenon of relaxation that is characterized by the reduction of stress with time, while total strain remains constant. Also, thermal steel creep is characterized by the fact that most of the deformations are irreversible even when the applied load is removed. Creep curves, defined as strain versus time curves, are typically divided into the three phases of primary, secondary, and tertiary as shown in Fig. 1. In the primary stage, the curve is non-linear and exhibits a decreasing creep strain rate. In the secondary stage, the creep strain is almost constant. In the tertiary stage, the creep strain rate increases with time. For steel, the shape of the creep curve, the magnitude of the creep strain and the time scale are highly dependent on both the temperature and the stress levels (Morovat et al. 2011 and Morovat et al. 2012).

B. Creep of ASTM A36 steel at elevated temperatures

Experimental and empirical models have been developed to predict creep strain of ASTM A36 steel at elevated temperatures (Harmathy 1967 and Fields and Fields 1989). One of the commonly used creep models in structural-fire engineering applications proposed by Fields and

Fields (Fields and Fields 1989) incorporates a power law creep and represents creep strain, ε_c , in the form of a Norton-Bailey equation (Norton 1929) as follows:

$$\varepsilon_c = at^b \sigma^c \quad (1)$$

In this equation, t is time and σ is stress. The parameters a , b and c are temperature-dependent material properties. Fields and Fields (Fields and Fields 1989) derived equations for these temperature-dependent material properties for ASTM A36 steel. The model developed by Fields and Fields (Fields and Fields 1989) is capable of predicting creep in the temperature range of 350 °C to 600 °C and for creep strains up to 6-percent. The creep model by Fields and Fields (Fields and Fields 1989) was used in the studies presented in this thesis on the time-dependent response of steel flush endplate connections to fire. The algorithm for creep strain rate was incorporated in ABAQUS via a user define subroutine.

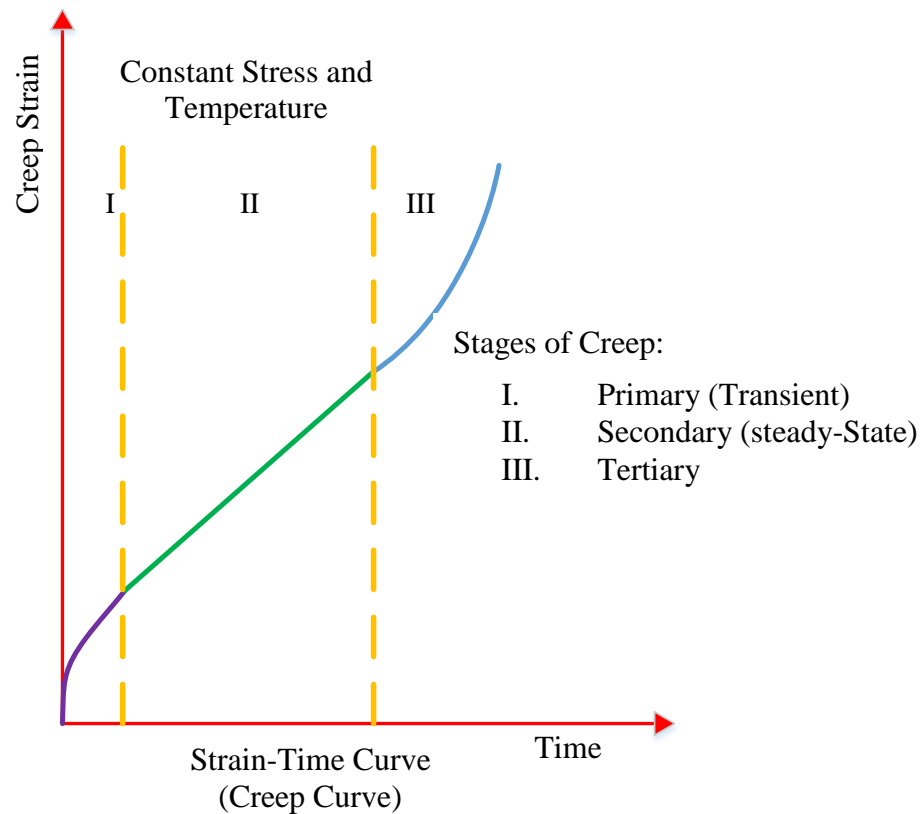


Fig. 1. Qualitative representation of creep curve for structural steel

CHAPTER III

THERMAL CREEP BEHAVIOR OF FLUSH ENDPLATE CONNECTIONS IN FIRE

A. Development of the FE modeling

In this section, a practical methodology developed to assess the time-dependent nature of the behavior of flush endplate beam-column connections in fire is presented. Time effects on the strength and rotational capacity of flush endplate connections are explicitly presented in the form of isochronous force-rotation curves.

1. Flush endplate connection prototype

The connection prototype selected for analysis followed the flush endplate connection details and design incorporated in the experiment conducted at University of Sheffield (2007). More specifically, as shown in Figs. 2 and 3, the flush endplate connection specimen used in the analysis consisted of a PL13×8×0.4 in. (PL323.4×200×10 mm) endplate, a W12×26 (UB305×165×40) beam, and a W10×60 (UC 254×254×89) column. Further, six grade 8.8 M20 bolts were used to connect the endplate to the column. Details of the connection configuration can be found in (University of Sheffield 2007; Al-Jabri et al. 2008; and Yu et al. 2011).

2. Boundary conditions

Boundary conditions are applied on the connection elements throughout the analysis. During the pretension step, all bolts are restrained against any translation to ensure contact between the bolt head and nut with the base material. During the loading step, the previous boundary condition is deactivated. The column was restrained against any translation and rotation throughout the analysis as shown in Fig.2.

3. Material properties and modeling considerations

An idealized bilinear stress-strain relation with isotropic hardening was used to model the mechanical behavior of both structural bolts and structural steel. The ambient temperature properties incorporated in connection simulations were based on the reported values in the experimental data at University of Sheffield (University of Sheffield 2007; Al-Jabri et al. 2008; and Yu et al. 2011). Retention factors proposed by researchers from the University of Texas at Austin (Lee et al. 2013) and University of Sheffield (Hu et al.2007) were used to respectively model stress-strain characteristics of structural steel and structural bolts at elevated temperatures. To account for the time-dependent behavior of structural steel at elevated temperatures, a power law creep model proposed by Fields and Fields (Fields and Fields 1989) was included in mechanical properties of structural steel used to model both the beam and the endplate. Thermal creep of structural bolts was ignored in connection simulations.

4. Model discretization

All the connection components are meshed with eight-node brick elements with reduced integration (C3D8-R) as shown in Fig.2. To improve the accuracy of predictions, a finer mesh is used around the connection region, where failure is likely to occur. Moreover, to account for stress concentration around the bolt-holes, a mapped meshing technique was used to discretize bolts and their surrounding areas. The surface interactions between the bolt shank, flush endplate, and the column flange are modeled using finite sliding, with a friction coefficient that changes with temperature.

B. Development of methodology

To develop the methodology, two series of FE analyses were performed using ABAQUS to investigate the effect of thermal creep on the behavior of flush endplate connection in real fire.

In the first series, steady-state temperature analyses were conducted to characterize the strength of flush endplate connections under combined shear and tension forces at elevated temperatures. At each specific temperature (450 °C, 550 °C, and 650 °C), an inclined concentrated force (with the initial angle of 35°) was monotonically applied to the beam end with an angle varying throughout the loading step in accordance with the experimental protocol at University of Sheffield (2007). Figure 4 shows sample results of such analyses where experimental and FE predictions of the strength of flush endplate connections are compared at various temperatures. As seen in Fig. 4 and as shown in previous studies (University of Sheffield 2007; Al-Jabri et al. 2008; and Yu et al. 2011), FE simulations are capable of predicting the experimental observations with reasonable accuracy. Also, Figs. 5 and 6 show a comparison of actual deformed shape and failure modes observed in the experiment of the flush endplate connection at 20 °C and 450°C against the corresponding FE simulations, respectively. It can be seen that the FE simulation can predict closely the excessive deformation that resulted in the endplate and the top bolts of the connection at 20 °C and endplate fracture at 450 °C. Note that due to the rapid loading protocol adopted in connection experiments at University of Sheffield (2007), the strengths obtained in the first series of simulations were assumed to be time-independent and therefore thermal creep of steel was ignored in these simulations.

In the second series, steady-state temperature creep tests were performed to investigate the creep response of flush endplate connections under combined shear and tension forces at elevated temperatures. More specifically, at each specific temperature (450 °C, 550 °C, and 650 °C), an

inclined force, equal to a fraction of the ultimate load predicted in the first series of analyses, was applied and kept constant throughout the test. Simulations were conducted for 240 minutes or until the connection failed. Note that Fields and Fields equations (Fields and Fields 1989) cannot predict accurately the creep behavior of steel at temperatures greater than 600 °C. Therefore, steady-state temperature creep tests at 650 °C were excluded from the analysis.

Then, same procedure was followed to examine the time-dependent behavior of the flush endplate connection under variable temperatures that ranges from at 450°C to 600 °C with 25°C increment. The ultimate loads predicted from the first series at each temperature are tabulated in table 1. It can be illustrated from the steady-state temperature analysis that for all temperatures greater than 450 °C the connection failure was governed by top bolt failure. Representative results of creep tests at different elevated temperatures that ranges from 450 °C to 600 °C with 25 °C and under various applied loads are shown in Figs. 7 to 13, respectively. Figures 7(a) and 7(b) represents the thermal creep behavior of flush endplate connection at 450 °C at different load ratio. It can be seen from Figs. 7(a) and 7(b) that the rate of increase in connection rotations is higher for larger applied loads and the connection cannot resist loads that are more than 90% of peak load for 240 min. Also, the failure mechanism of flush endplate connection at 450 °C changes from endplate failure to tension bolt failure at 95% of peak load due to stress relaxation in the endplate and induced tensile stresses generation in the tension bolts. Moreover, Figs. 8 to 13 describe the thermal creep behavior of flush endplate connection at temperatures ranges from 475 °C to 600 °C with 25 °C increment at different load ratios. The results show that flush endplate connection cannot resist loads greater than 85%, 80%, 75%, 70%, 65%, 65% of peak loads estimated from the steady-state temperature analysis at 475 °C, 500 °C, 525 °C, 550 °C, 575 °C, 600 °C, respectively. This indicates that as thermal creep is explicitly considered in the beam and the end plate materials,

the connection rotation increases with time therefore generating induced tensile stresses in the top bolts, and consequently leading to tension bolt failure.

Results obtained from steady-state temperature creep tests in the form of rotation versus time, can alternatively be presented in the form of isochronous force-rotation curves. Figure 14 shows a sample of isochronous force-rotation curves at 550 °C corresponds to the creep test results shown in Fig. 11. As can be seen in Fig.14, for any specific temperature like 550 °C, isochronous force-rotation curves are force-rotation curves at different time. In other words, they represent the time-dependent force-rotation response of the connection at any specific temperature. As further observed in Fig. 14, compared to a single curve from connection experiments, isochronous force-rotation curves provide much richer insight into the connection behavior at elevated temperatures. It can be seen that at a specific time, larger connection rotation can be obtained for larger applied load.

C. Application of methodology

The methodology presented in the previous section to assess the time-dependent behavior of flush endplate connections subjected to fire temperatures can be used to study the behavior of flush endplate connections under more general conditions and characteristics of buildings in fire.

Steady-state temperature creep analysis, as explained previously, can be performed on the isolated flush endplate connection model in ABAQUS under a constant applied load at different temperatures. Such analysis can be used to develop a transient thermal creep analysis by developing isochronous rotation-temperature curves to evaluate the effect of creep on the performance of flush endplate connections in a real fire. A representative of these isochronous rotation-temperature curves for a constant load of 76 kN is depicted in Fig. 15 where 76 kN

represents the peak load resulting from the steady-state temperature analysis at 600 °C. The isochronous rotation-temperature curves such as the ones shown in Fig. 15 simply indicate the time-dependent behavior of the flush endplate connections under transient temperature conditions characteristics of structural fires. It can be seen that for temperatures greater than 540 °C, tension bolt failure governs the behavior of the connection, and the connection resistance decreases linearly for less time durations as temperature increases.

The connection rotation versus temperature shown in Fig.15 is presented in a more general form as shown in Fig. 16. Figure 16 is a 3D graph representation that indicates a transient temperature creep analysis that can evaluate the effect of creep on the performance of flush endplate connection in real fires or in various fire rate scenarios. In other words, for any fire rate scenario, the total connection rotation can be predicted as load is kept constant and temperature is varying with time.

Furthermore, the graphs shown in Fig. 15 can also be represented in a way where the time-dependent behavior of flush endplate connections is presented under the conditions of variable loads and temperatures. Samples of such general isochronous rotation-temperature curves are shown in Figs. 17(a) and 17(b). Note that even though curves in Figs. 17(a) and 17(b) correspond to 0.8 of the ultimate loads and half of ultimate loads at each temperature, respectively, the actual loads are different from one temperature to the other (ultimate loads are the peak loads predicted in the first series of analyses where the creep effects are ignored). An important observation from Figs. 15, 16, and 17 is that, according to the adopted creep model by Fields and Fields (Fields and Fields 1989), the behavior of the selected flush endplate connection becomes highly time-dependent for temperatures above 500 °C. Figures 17(a) and 17(b) further show that creep effect on the connection response to fire becomes more significant at higher applied loads.

Any time and temperature point on the isochronous rotation-temperature curves in Figs. 15, 16, and 17 can be related to a corresponding point on the design fire curve. This correspondence allows a designer to define the desirable performance levels for steel connections in terms of specific times or temperatures. In other words, the isochronous representations shown in Figs. 15, 16, and 17 can be utilized to define critical times and temperatures for designing connections in fire. This utilization can further provide a smooth transition from the current prescriptive-based approaches to the performance-based ones.

Table 1. Ultimate loads predicted from steady-state temperature analysis at different elevated temperatures

Temperature (°C)	Tension (kN)	Shear (kN)	Total Load (kN)
450	131.2	109.7	171
475	115.4	93.2	148.4
500	101.3	81.4	129.9
525	91.3	73	116.9
550	75.7	65.2	99.9
575	68.7	54.5	87.7
600	59.3	47	75.7
650	30.4	27.3	40.8

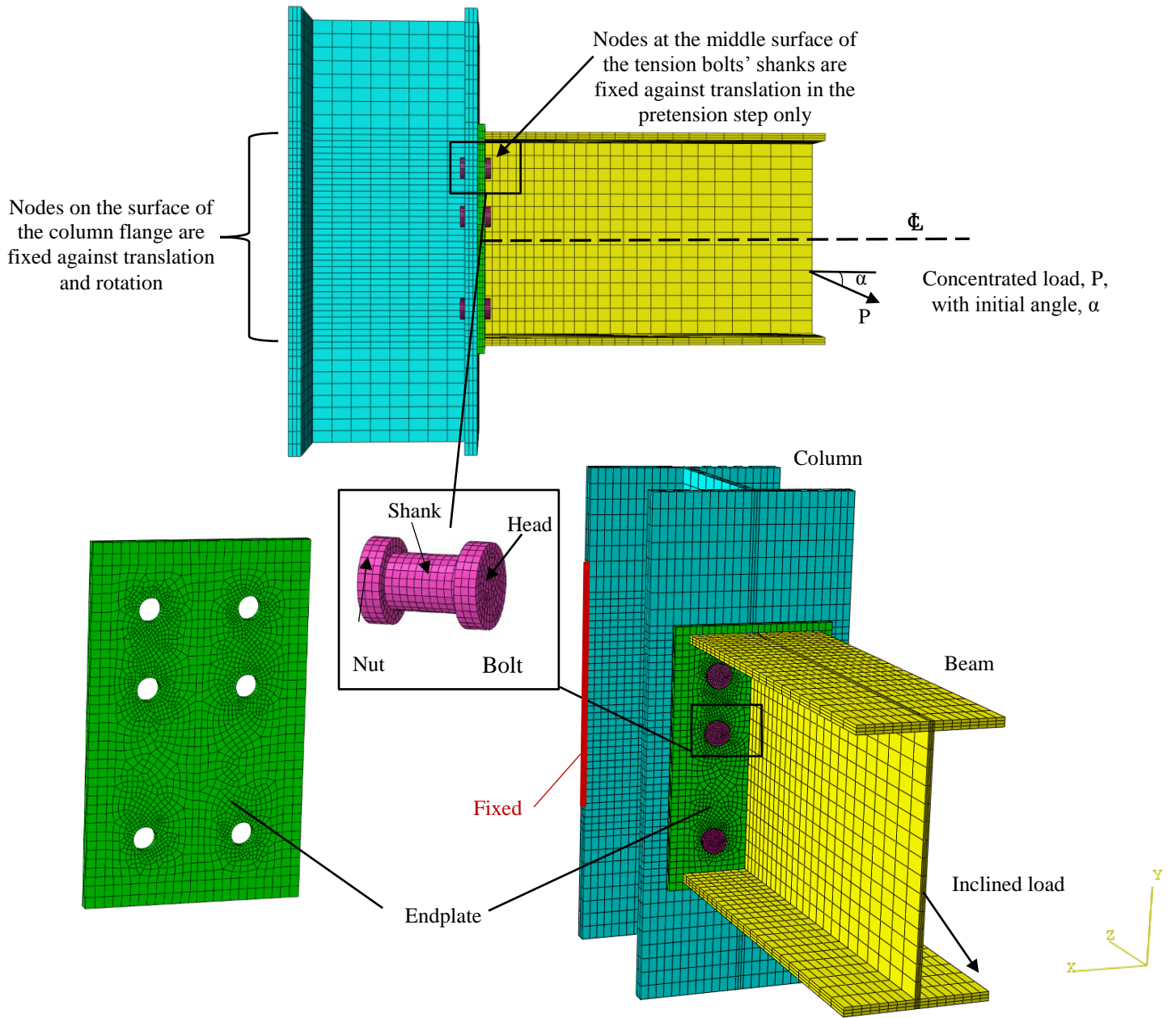


Fig. 2. Flush endplate connection configuration used in simulations in ABAQUS.

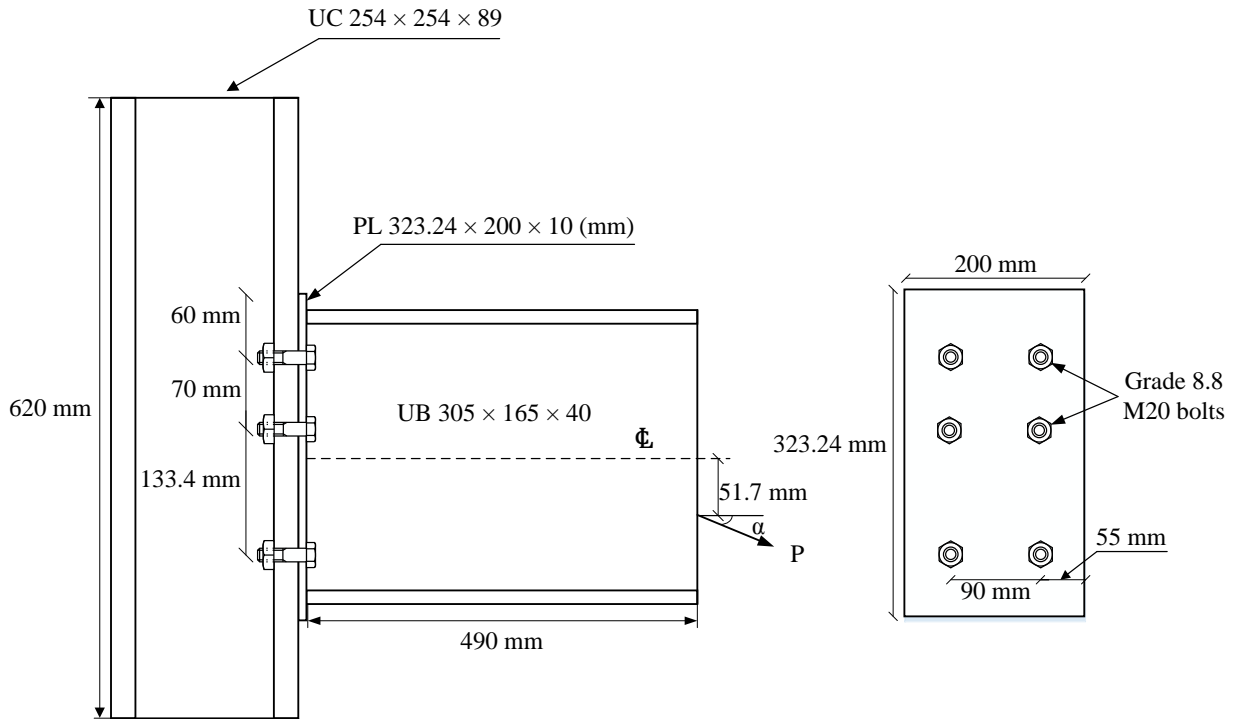


Fig. 3. Flush endplate connection configuration utilized in the study.

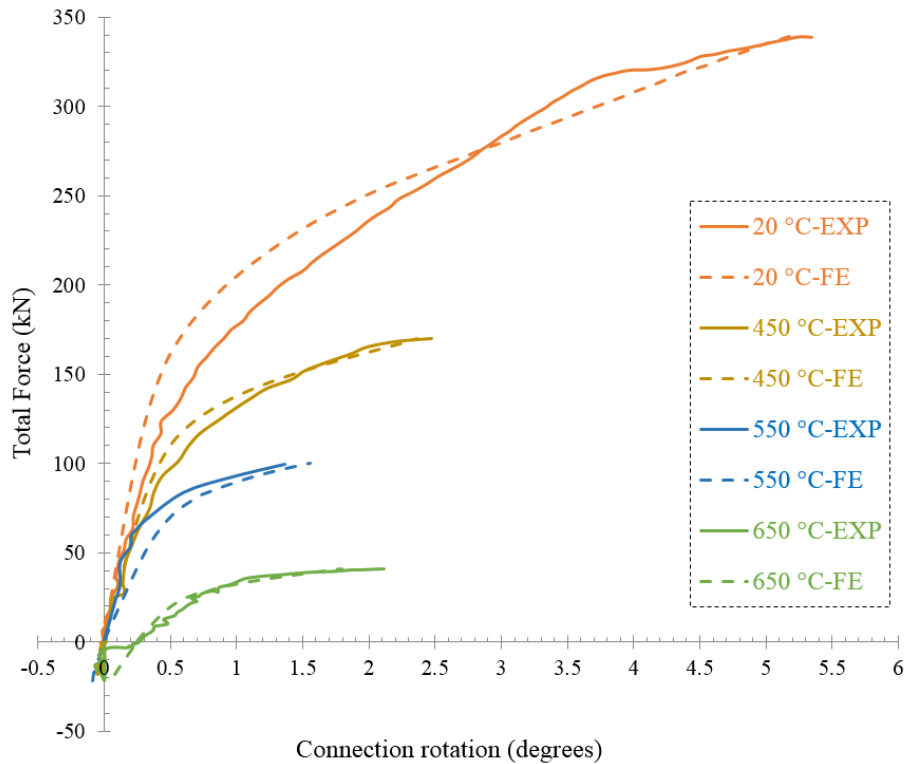


Fig. 4. Time-independent strength of flush endplate connections at ambient and elevated temperatures.

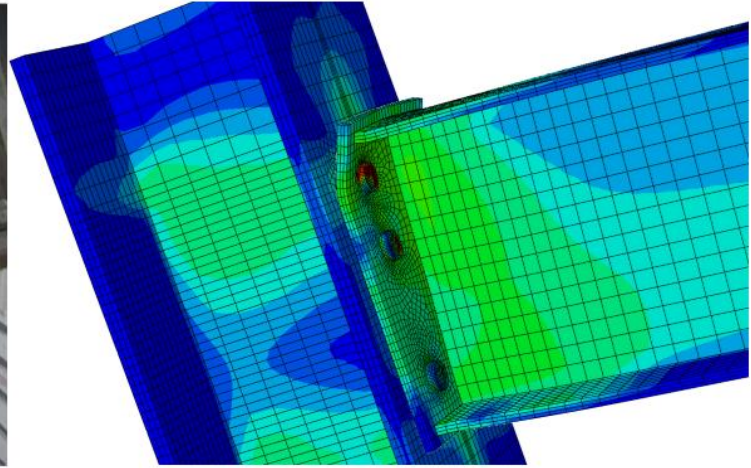


Fig. 5. Time-independent connection deformation of flush endplate connections at 20°C

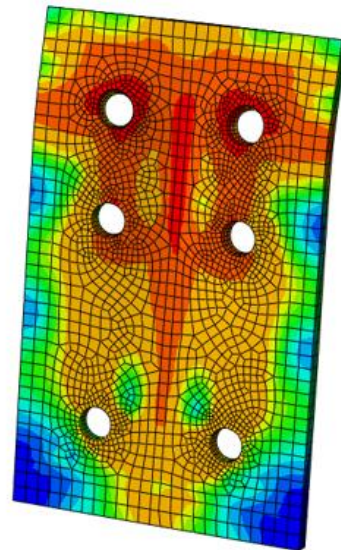
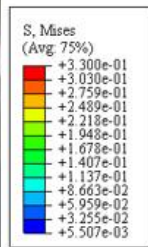
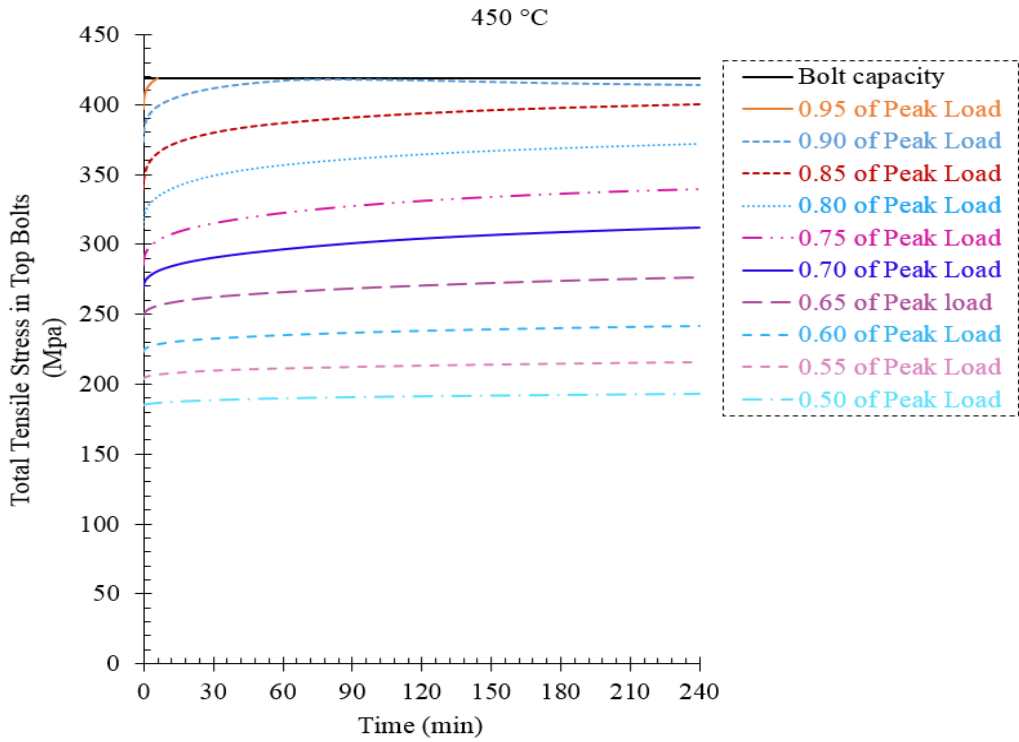
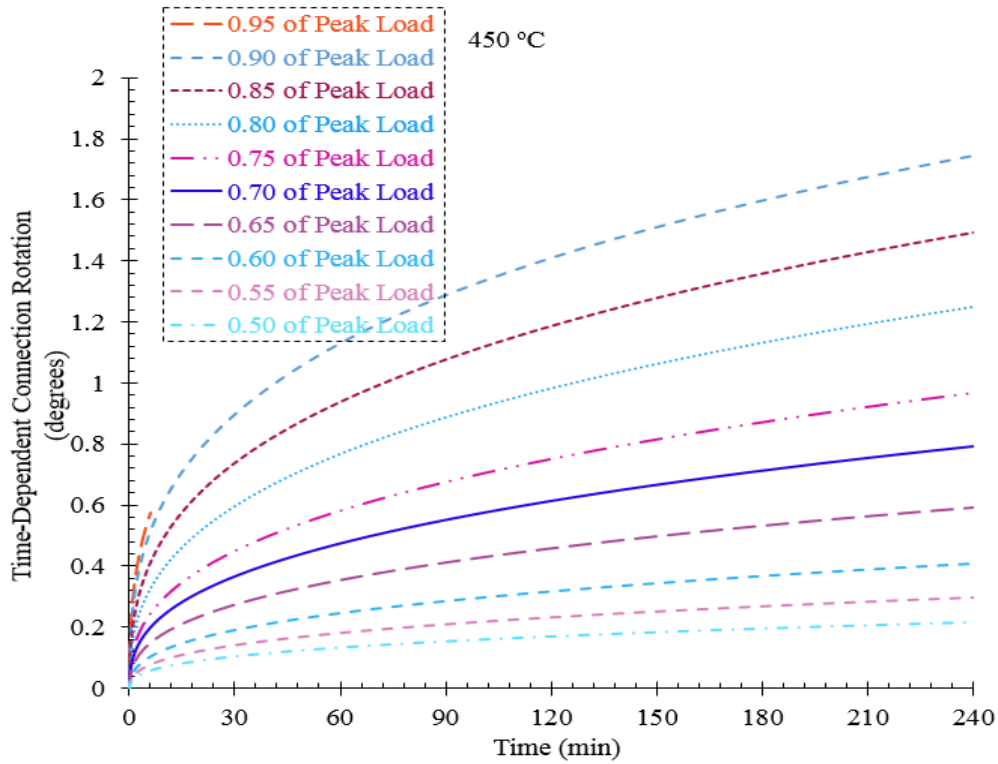


Fig. 6. Time-independent endplate deformation of flush endplate connections at 450°C



(a)



(b)

Fig. 7. Thermal creep behavior of flush endplate connection at 450 °C: (a) Total tensile stress in top bolts vs. time, (b) Connection rotation vs. time.

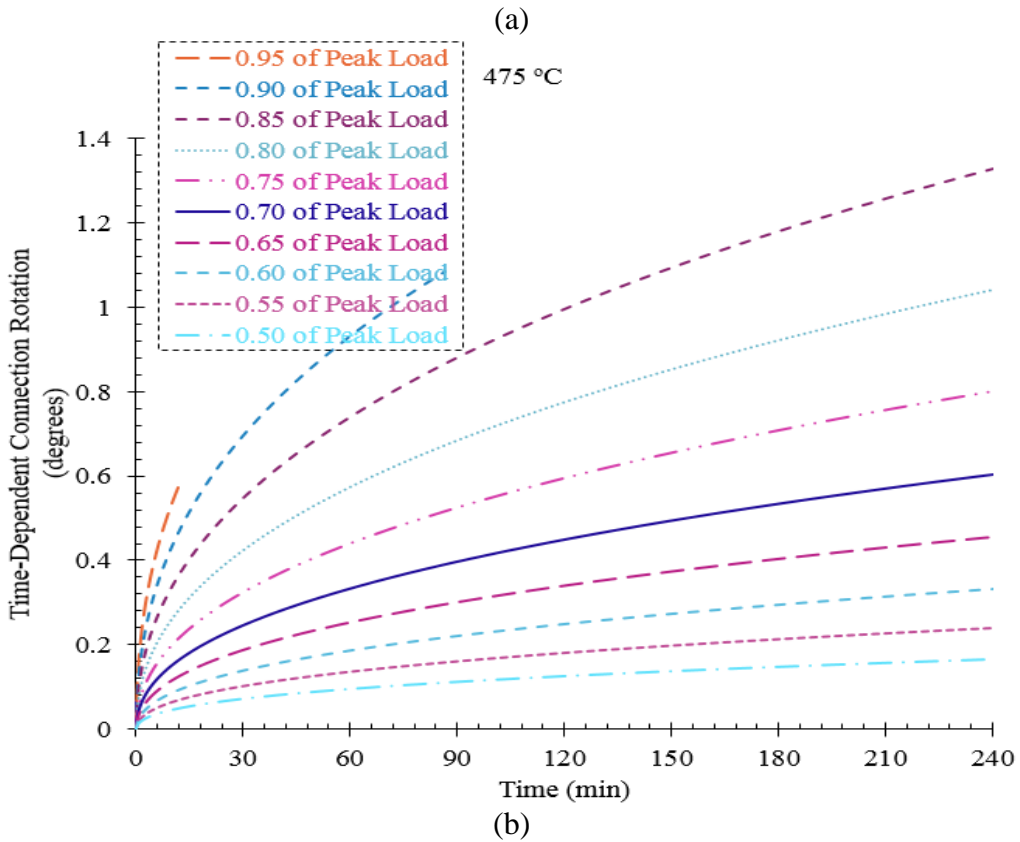
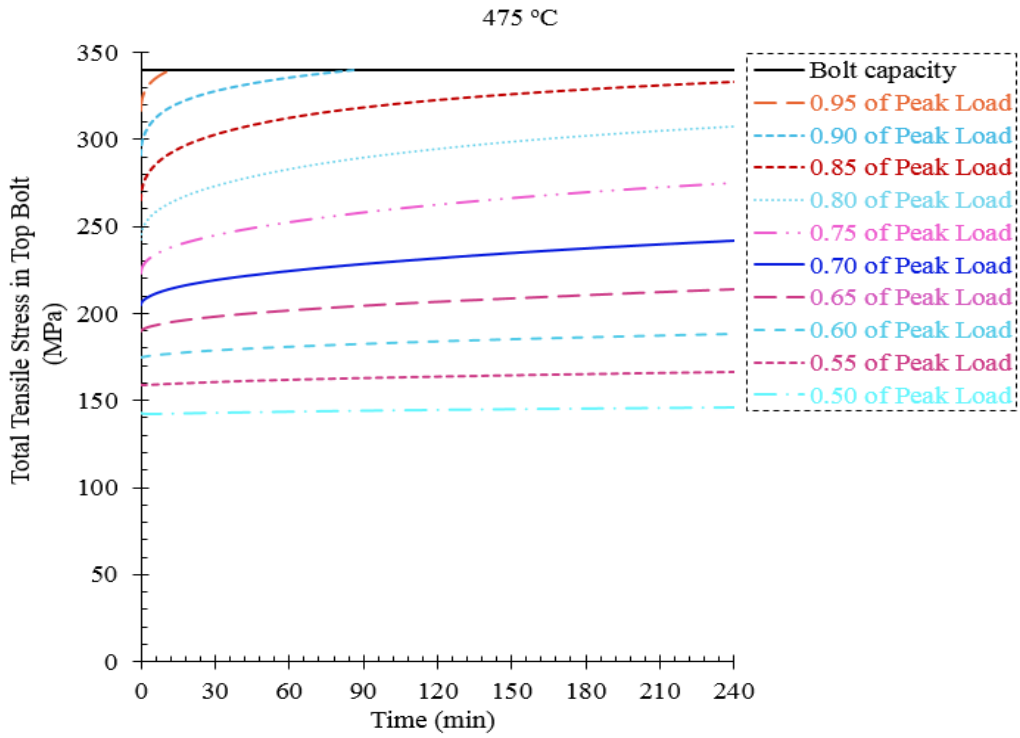
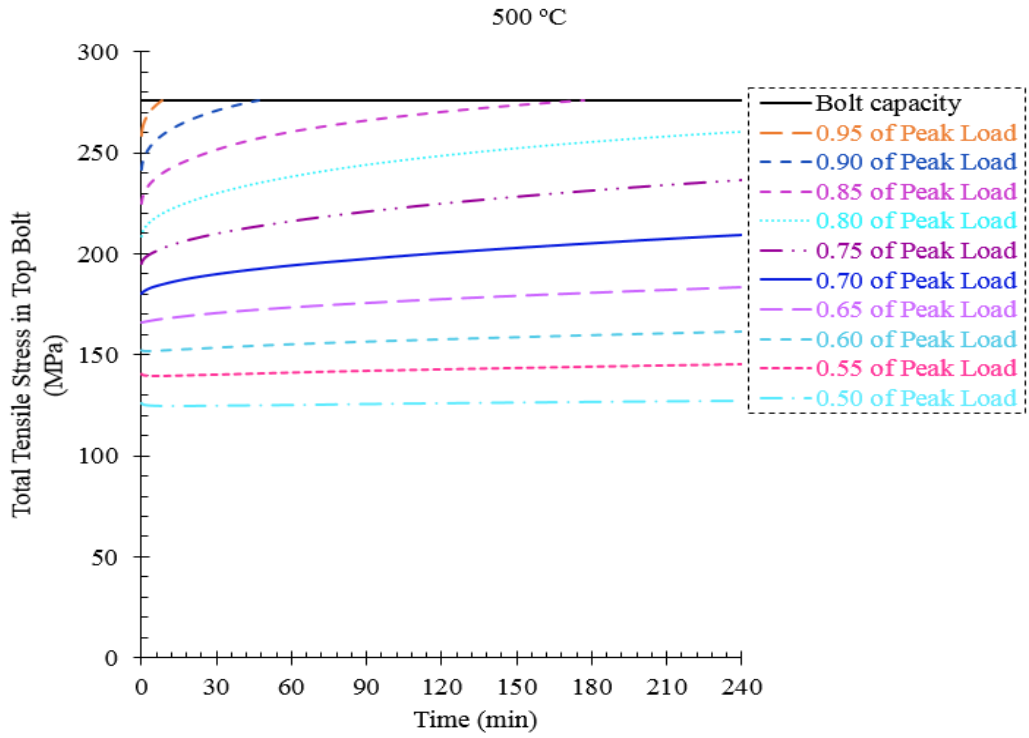
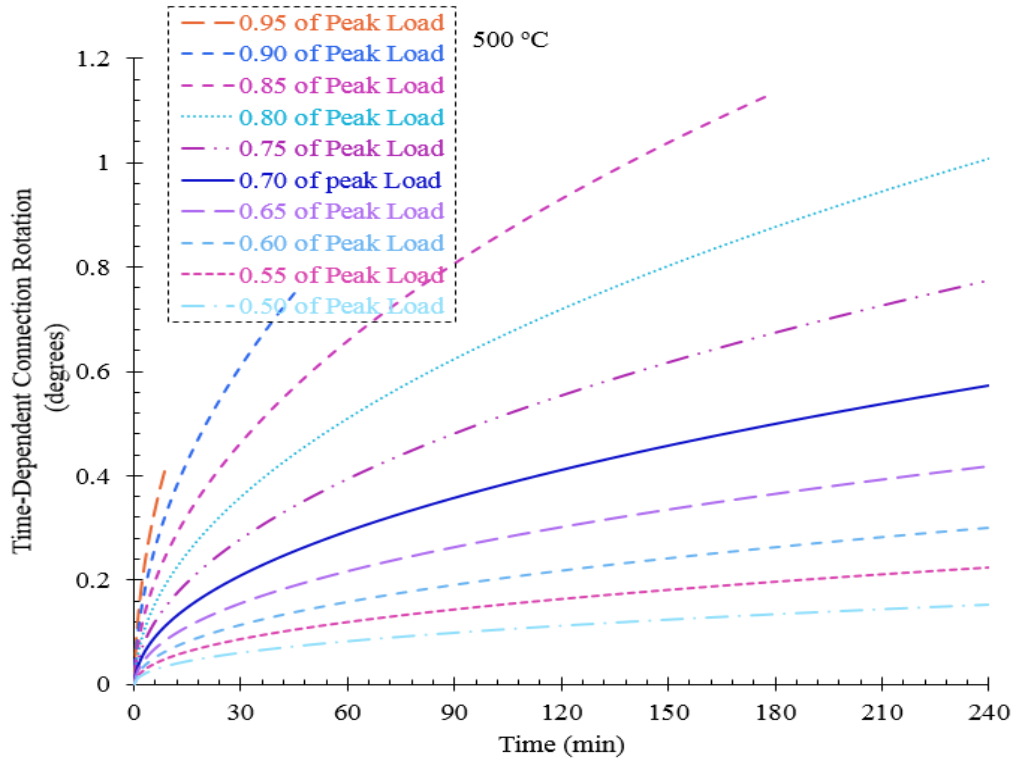


Fig. 8. Creep behavior of flush endplate connection at 475 °C: (a) Total tensile stress in top bolts vs. time, (b) Connection rotation vs. time.

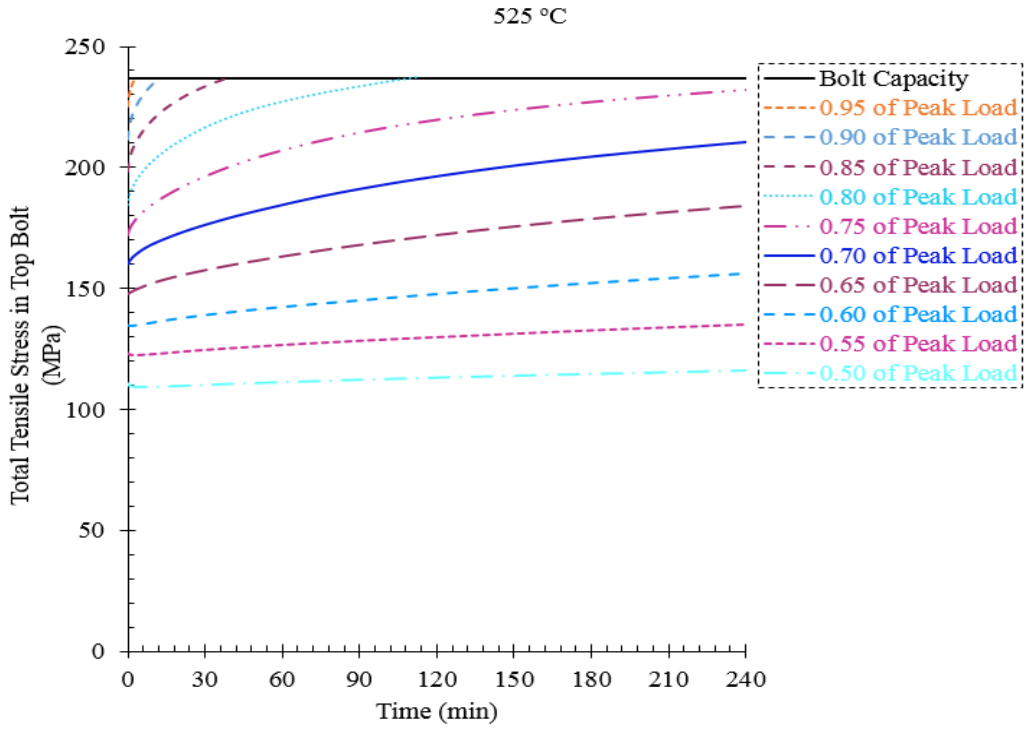


(a)

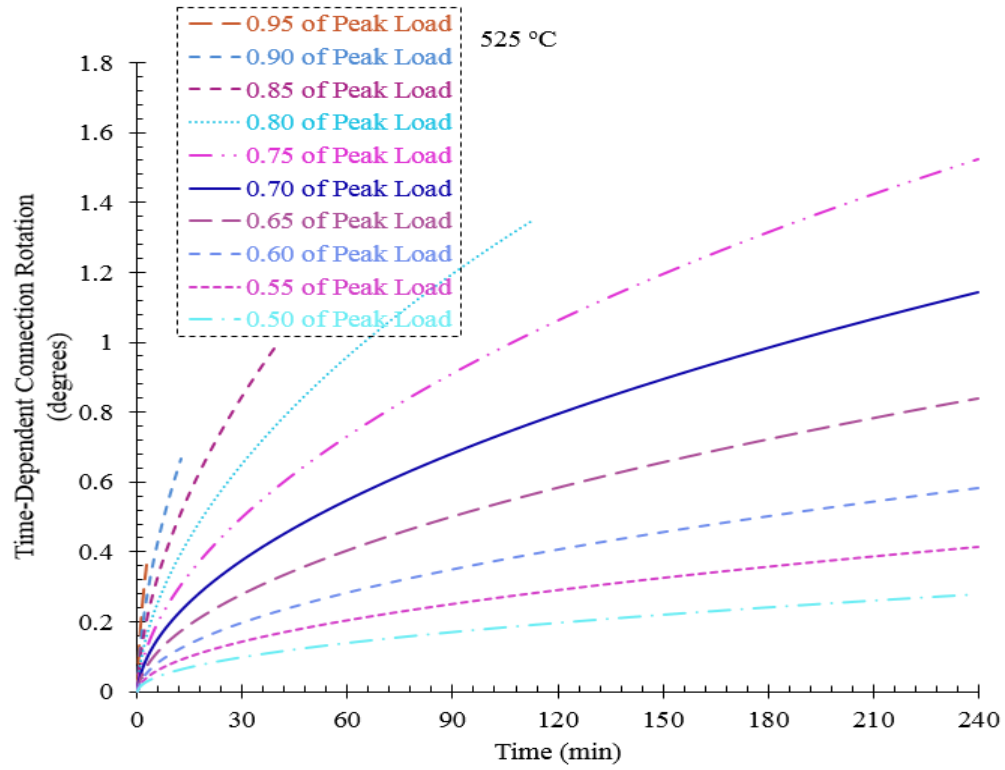


(b)

Fig. 9. Thermal creep behavior of flush endplate connection at 500 °C: (a) Total tensile stress in top bolts vs. time, (b) Connection rotation vs. time.

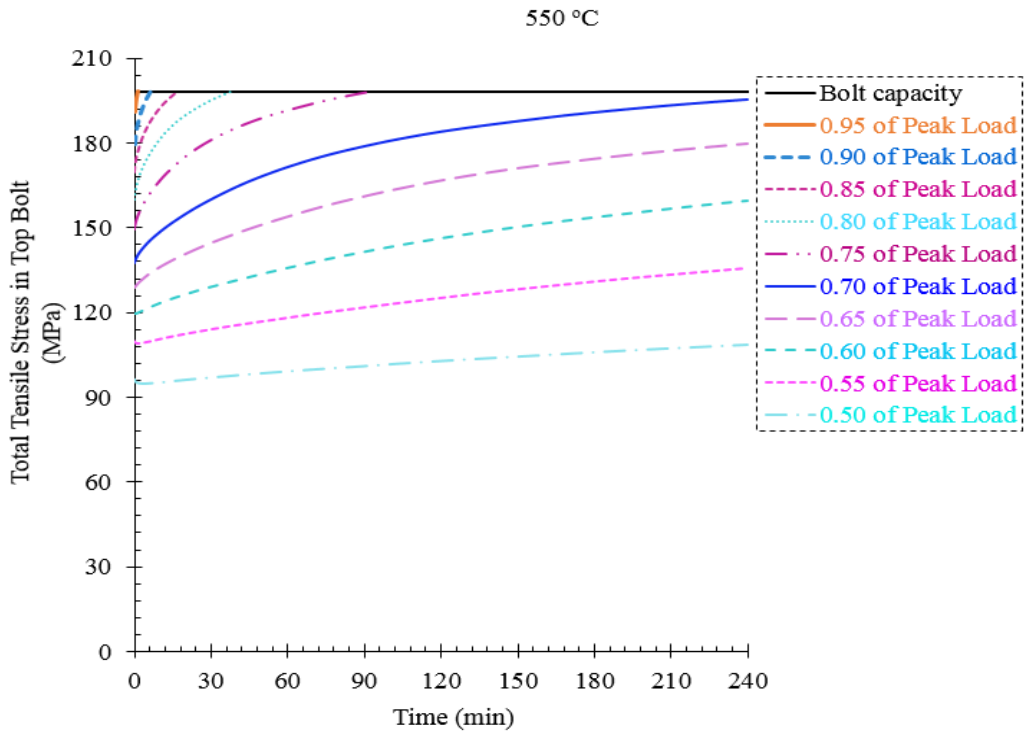


(a)

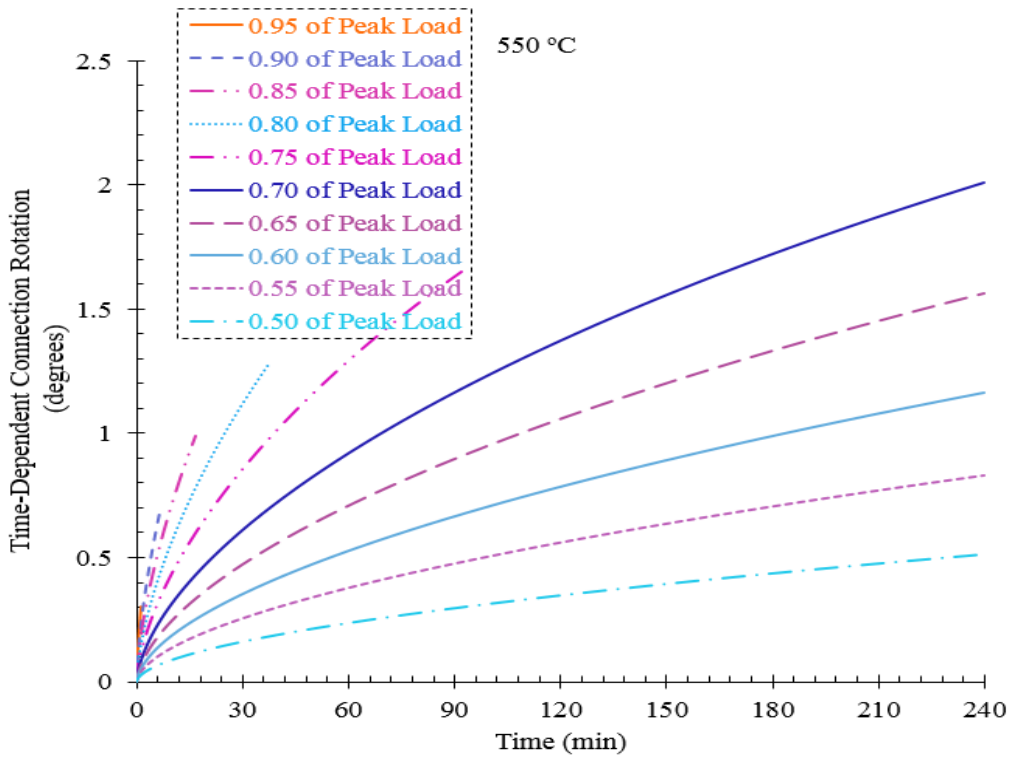


(b)

Fig. 10. Thermal creep behavior of flush endplate connection at 525 °C: (a) Total tensile stress in top bolts vs. time, (b) Connection rotation vs. time.

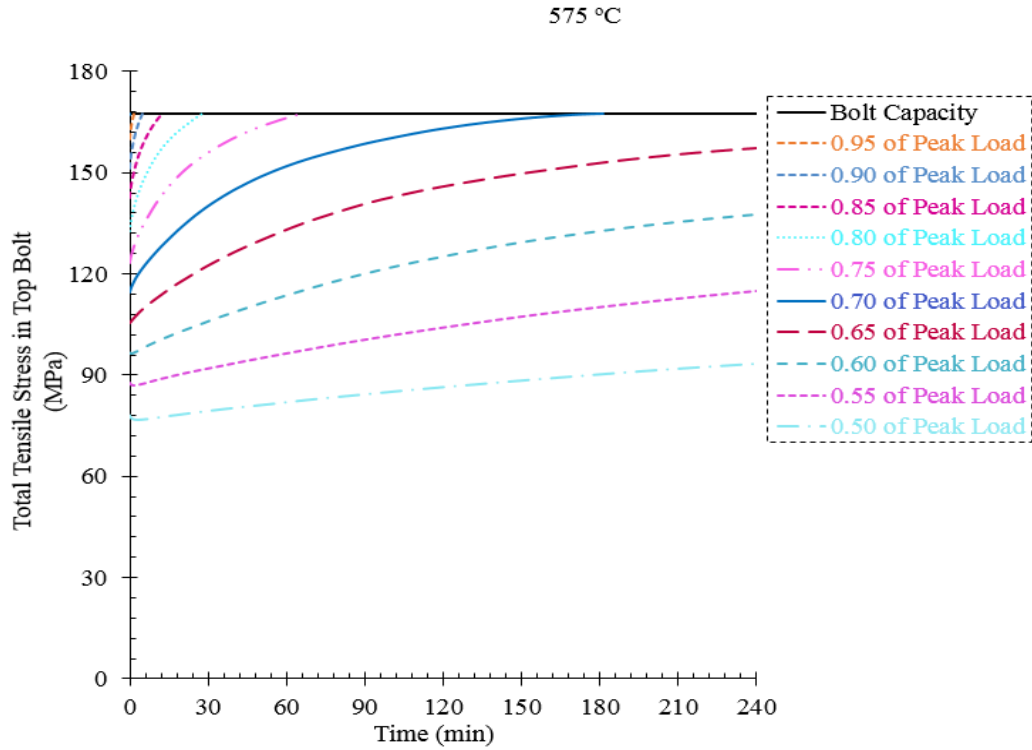


(a)

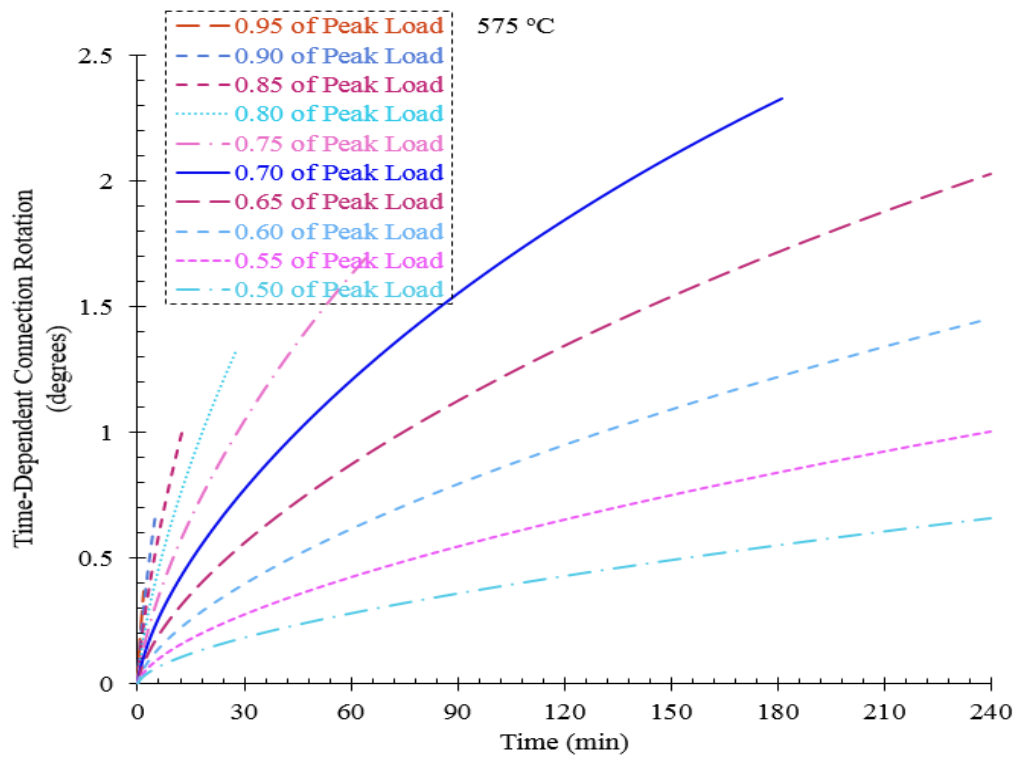


(b)

Fig. 11. Thermal creep behavior of flush endplate connection at 550 °C: (a) Total tensile stress in top bolts vs. time, (b) Connection rotation vs. time.

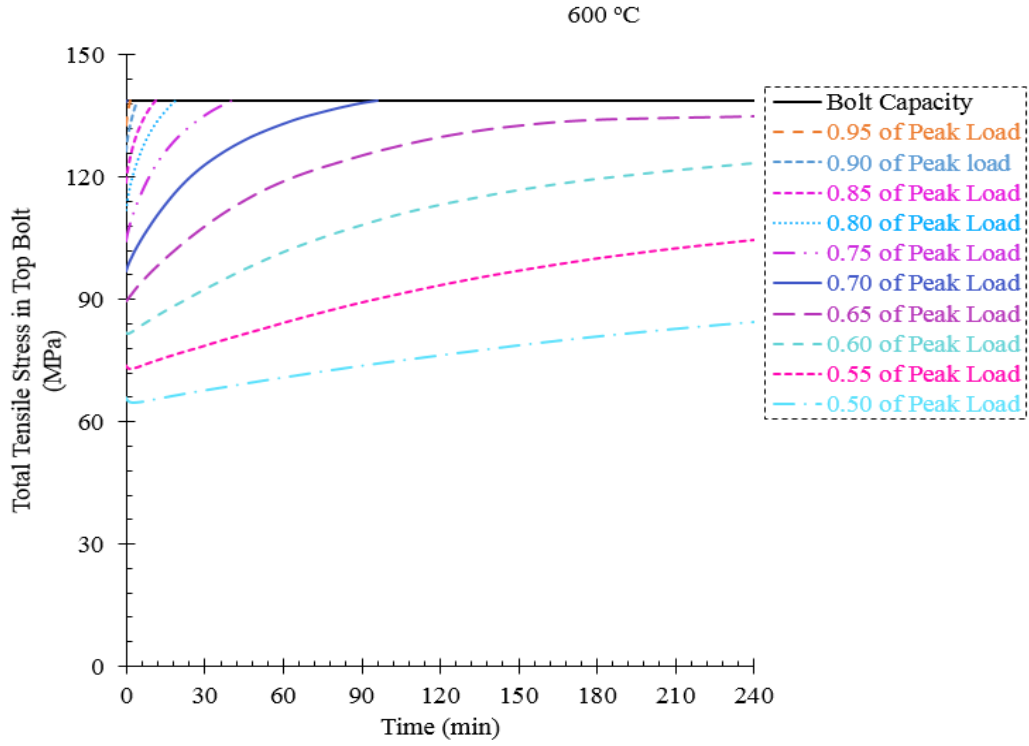


(a)

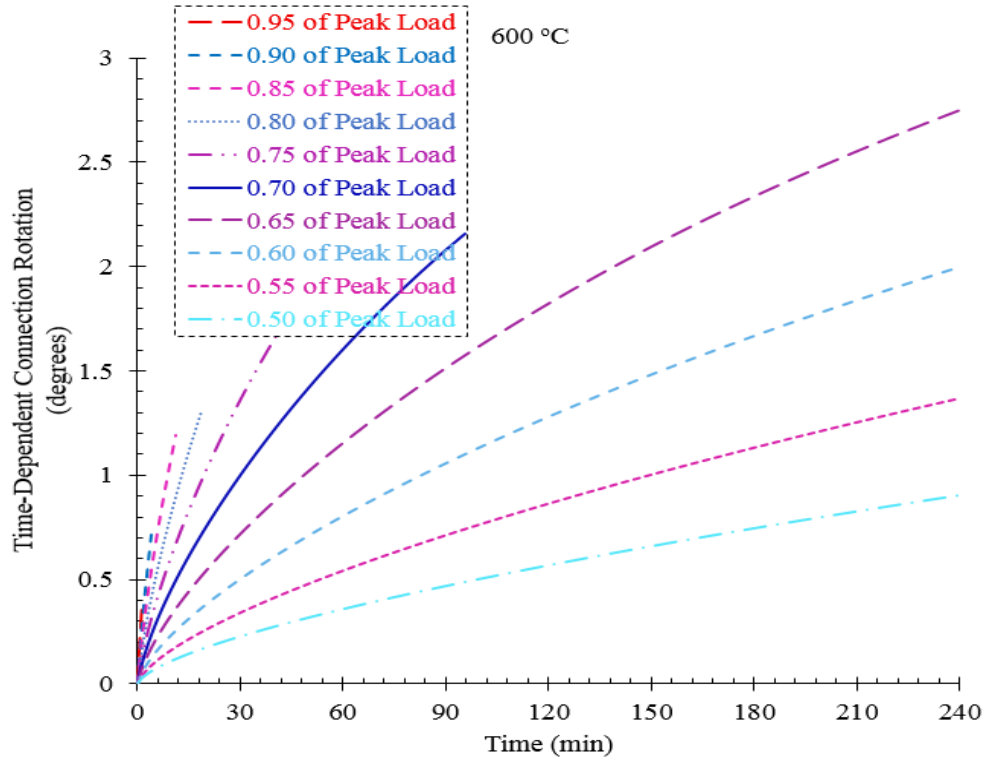


(b)

Fig. 12. Thermal creep behavior of flush endplate connection at 575 °C: (a) Total tensile stress in top bolts vs. time (b) Connection rotation vs. time.



(a)



(b)

Fig. 13. Thermal creep behavior of flush endplate connection at 600 °C: (a) Total tensile stress in top bolts vs. time, (b) Connection rotation vs. time.

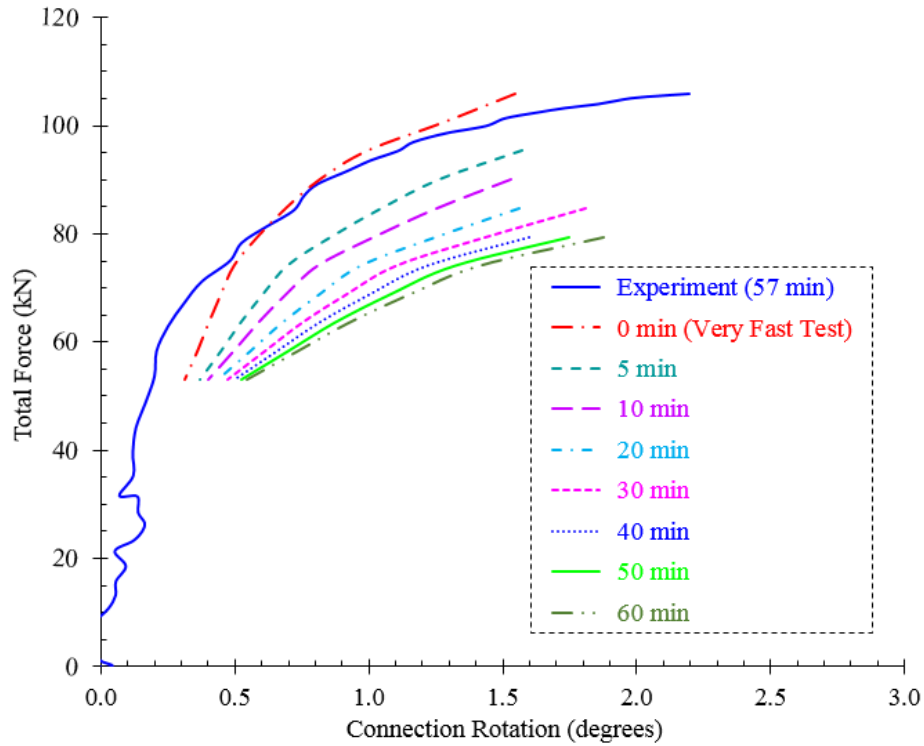


Fig. 14. Isochronous force-rotation curves for the flush endplate connection in consideration at 550°C

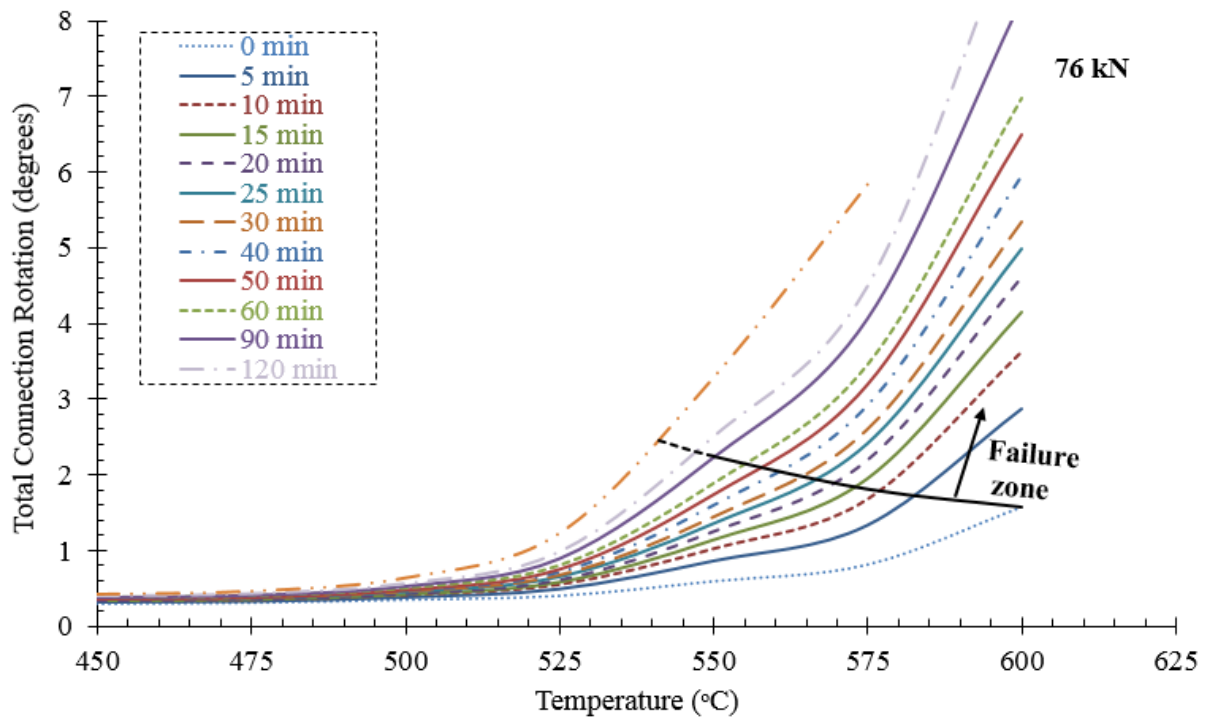


Fig. 15. Isochronous rotation-temperature curves corresponding to the constant load of 76 kN

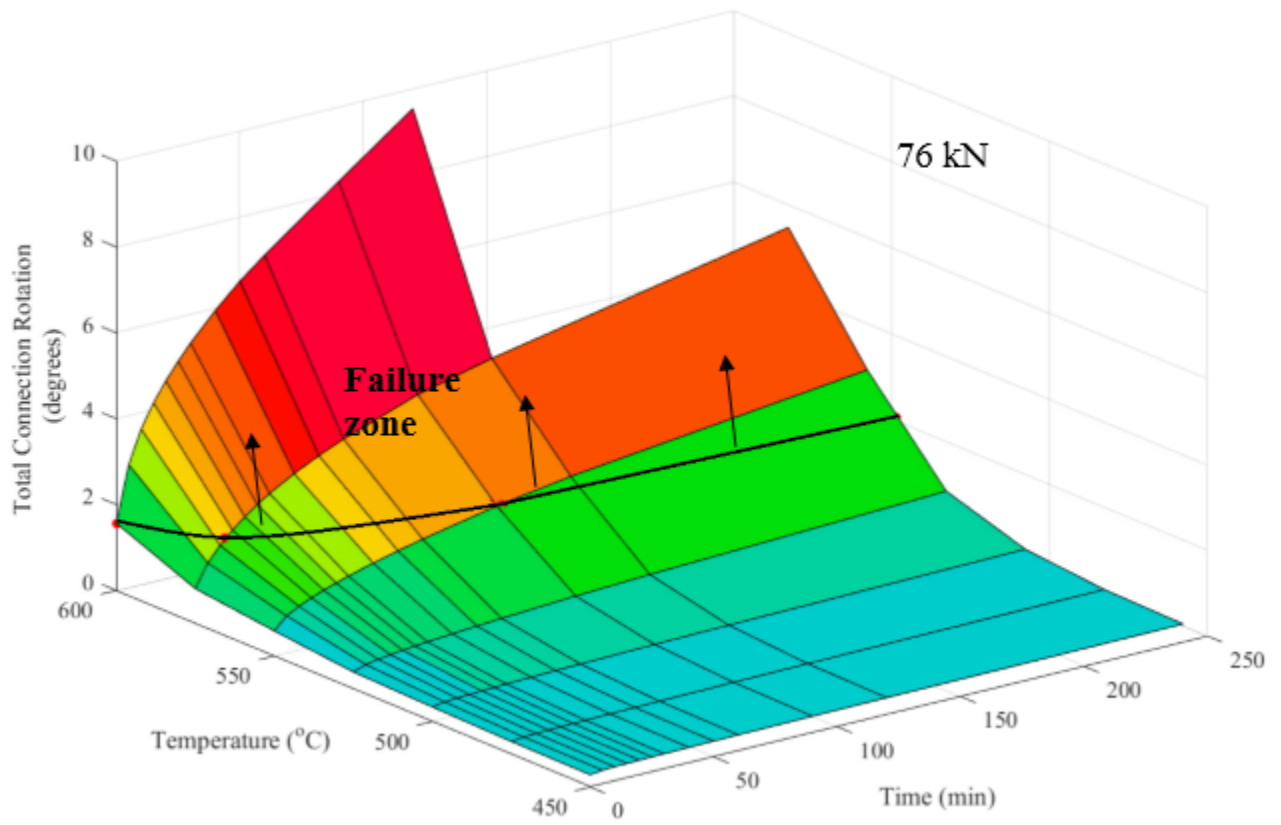
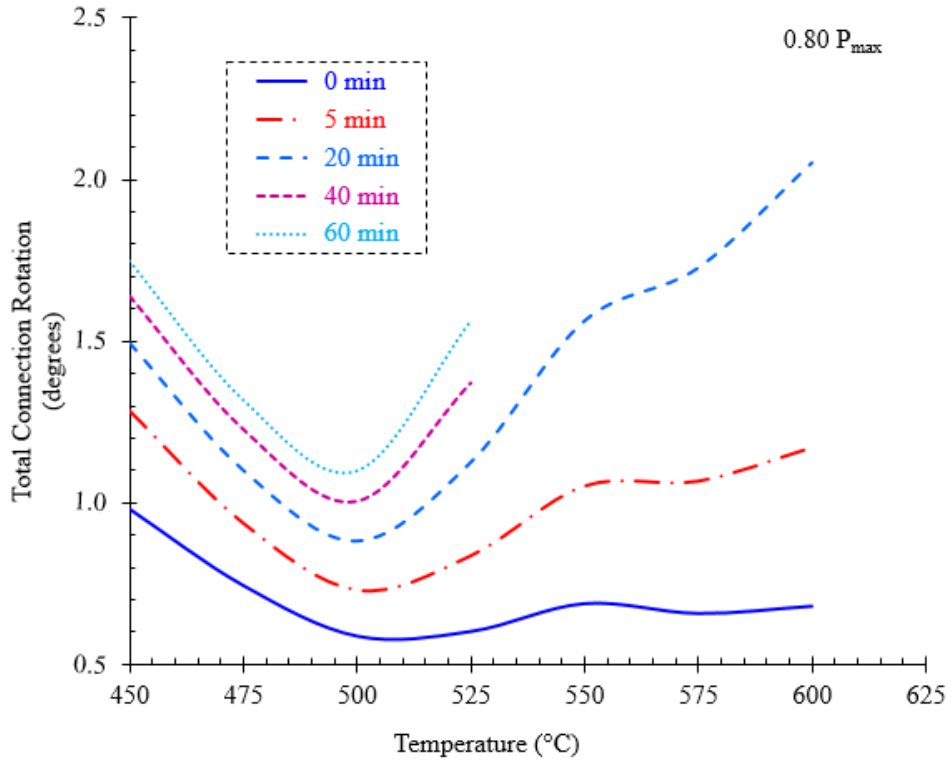
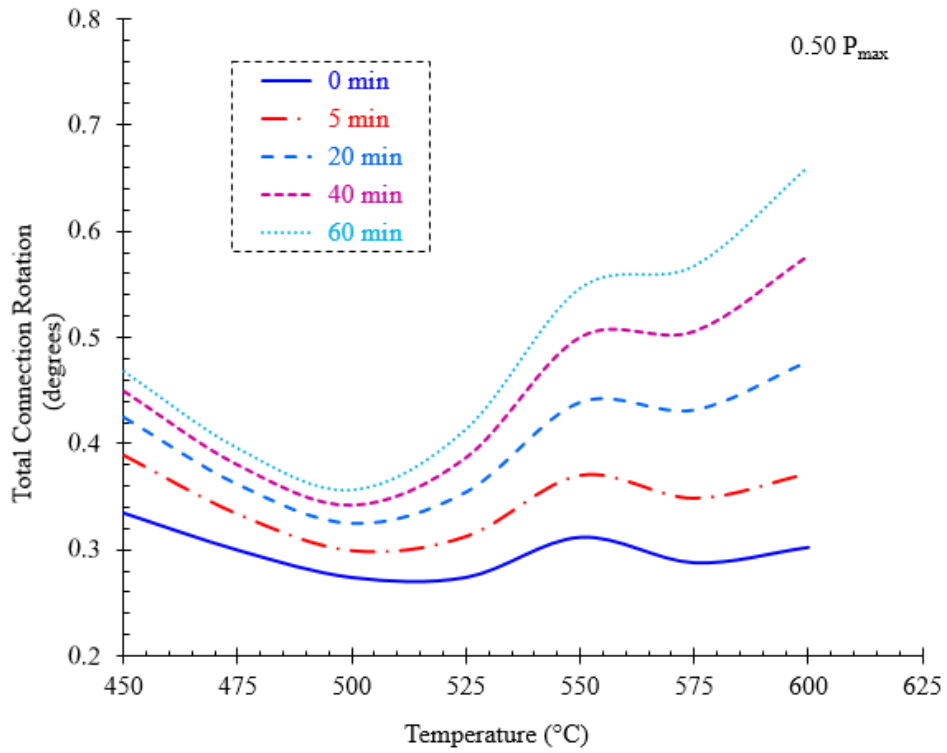


Fig. 16. 3D Representation of isochronous rotation-temperature curves corresponding to the constant load of 76 kN



(a)



(b)

Fig. 17. Isochronous rotation-temperature curves under variable loads

CHAPTER IV

PARAMETERS AFFECTING THE TIME-DEPENDENT BEHAVIOR

A. Parameters affecting the time-dependent behavior of flush endplate connections in fire

The methodology explained previously can be used to examine the effect of some major geometrical parameters such as different load angles, endplate thicknesses, bolt diameter, and different plate thickness with different bolt diameter on the time-dependent behavior of flush endplate connections subjected to fire.

1. Load angle

A Steady-state temperature analysis was conducted first to characterize the strength of flush endplate connections under combined shear and tension forces at elevated temperatures (475 °C, 550 °C, and 600 °C) with different initial load angles (35°, 45°, and 55°). Then, a steady-state temperature creep analysis was conducted to investigate the effect of different load angles on the time-dependent behavior of flush endplate connections. Three different load to peak load ratios (1.00, 0.70, and 0.50) were incorporated in steady-state temperature creep analysis regardless the occurrence of failure or not as shown in Fig. 18. It can be seen from Fig. 18 that the variation of load angle does not affect significantly the time-dependent behavior of flush endplate connections. However, for peak loads, the time-dependent connection rotation slightly increases as the load angle increases. The reason behind is that as the load angle increases the shear load applied at the tip of the beam increases whereas the tension load decreases consequently. However, the combined shear and tension loads give approximately similar applied moment on the beam end connection

that leads the connection to behave similarly for different load angles at the same temperature when thermal creep is explicitly considered in the connection.

2. Endplate thickness

Another parameter incorporated in this study is the effect of endplate thickness on the time-dependent behavior of flush endplate connections in fire. A steady-state temperature analysis was conducted first on ABAQUS to identify the peak load that flush endplate connection with 8 mm endplate thickness can withstand at different elevated temperatures (475 °C, 550 °C, and 600 °C). The loads resulting from the steady-state temperature analysis at 475 °C, 550 °C, 600 °C are 130 kN, 83 kN, and 56 kN, respectively. Note that for 475 °C, the connection failure was controlled by endplate fracture, whereas tension top bolt failure controlled the behavior of the connection at 550°C and 600 °C. Then, a steady-state creep analysis was conducted to investigate the effect of different endplate thicknesses (8 mm, 10 mm, and 15 mm) on time-dependent behavior of the flush endplate connection under the same load identified in steady-state temperature analysis. The results are illustrated in Fig. 19. It can be seen that for all temperatures (475 °C, 550 °C, and 600 °C) the time-dependent creep strain increases as the endplate thickness decreases. The slender the endplate is, the larger rotation can be resulted due to creep effect on the connection when both temperature and load are kept constant.

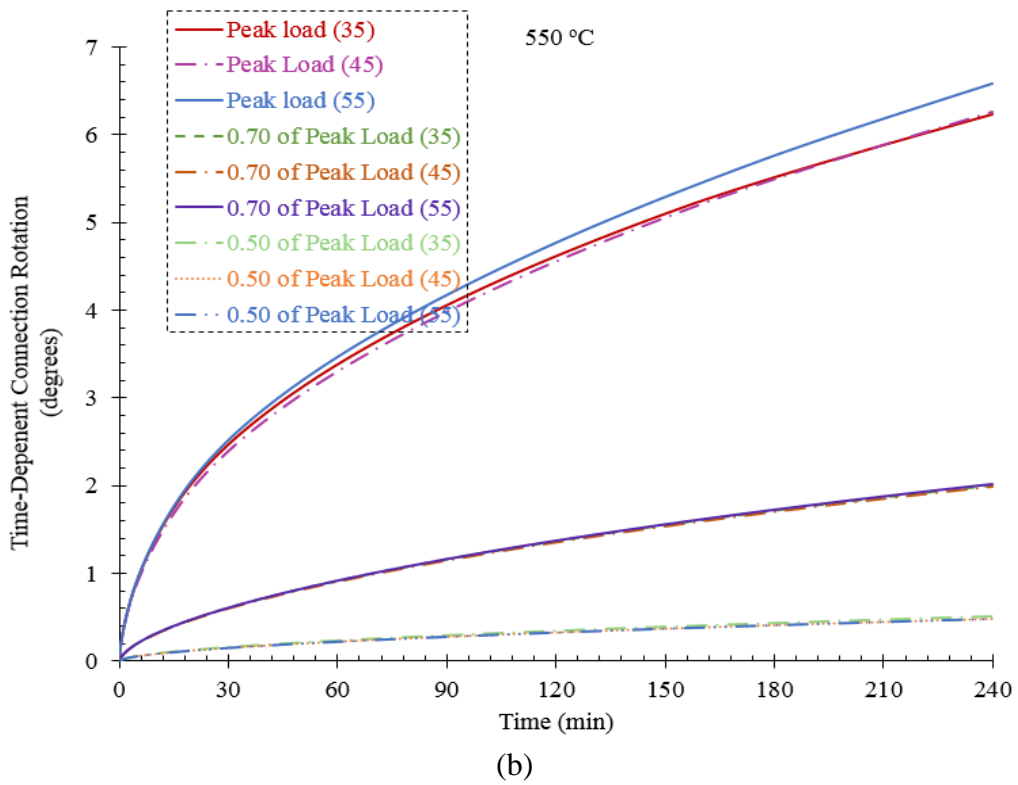
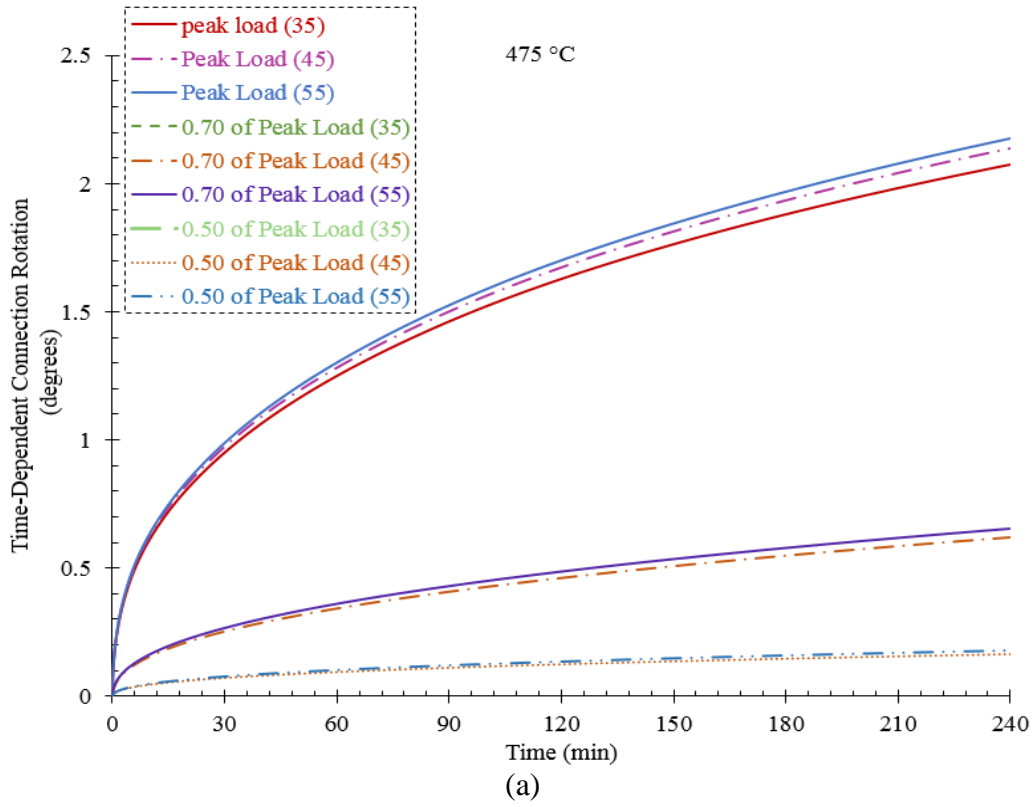
3. Bolt diameter

Same methodology was conducted to investigate the effect of different bolt diameters on the thermal creep behavior of flush endplate connections at elevated temperatures due to fire. Grade 8.8 M27 bolts were used in this analysis to ensure the occurrence of endplate failure in the steady-state temperature analysis. Figures 20 and 21 illustrate the creep behavior of flush endplate connection having M27 bolts at 550 °C and 600 °C, respectively. It can be seen that flush endplate

connection cannot withstand loads greater than 90% and 75% of peak loads at 500 °C and 600 °C, respectively. Note that the FE simulations at 600 °C were conducted for 120 min or until the connection failed. Figures 22(a) and 22(b) indicate the stress relaxation in the endplate at 500 °C and 600 °C when 90% of the peak load is applied, respectively. The figures show that as thermal creep is explicitly considered, the endplate undergoes stress relaxation with excessive deformation that leads to tension bolt failure.

4. M27 bolt with 8 mm endplate thickness

The developed methodology was also used to investigate the thermal creep behavior of flush endplate connection with six grade 8.8 M27 bolts with 8mm endplate thickness at 500 °C. In steady-state temperature analysis the connection behavior was controlled by endplate failure due to its slenderness. However, in steady-state creep analysis the stresses in the beam and endplate tend to relax that result in increasing connection rotation and generating higher tensile stress in the top tension bolts as shown in Figs. 23(a) and 23(b). It should be noted that the results show that the induced tensile stresses in top bolts do not reach the tension bolt capacity due to the early failure of the slender endplate.



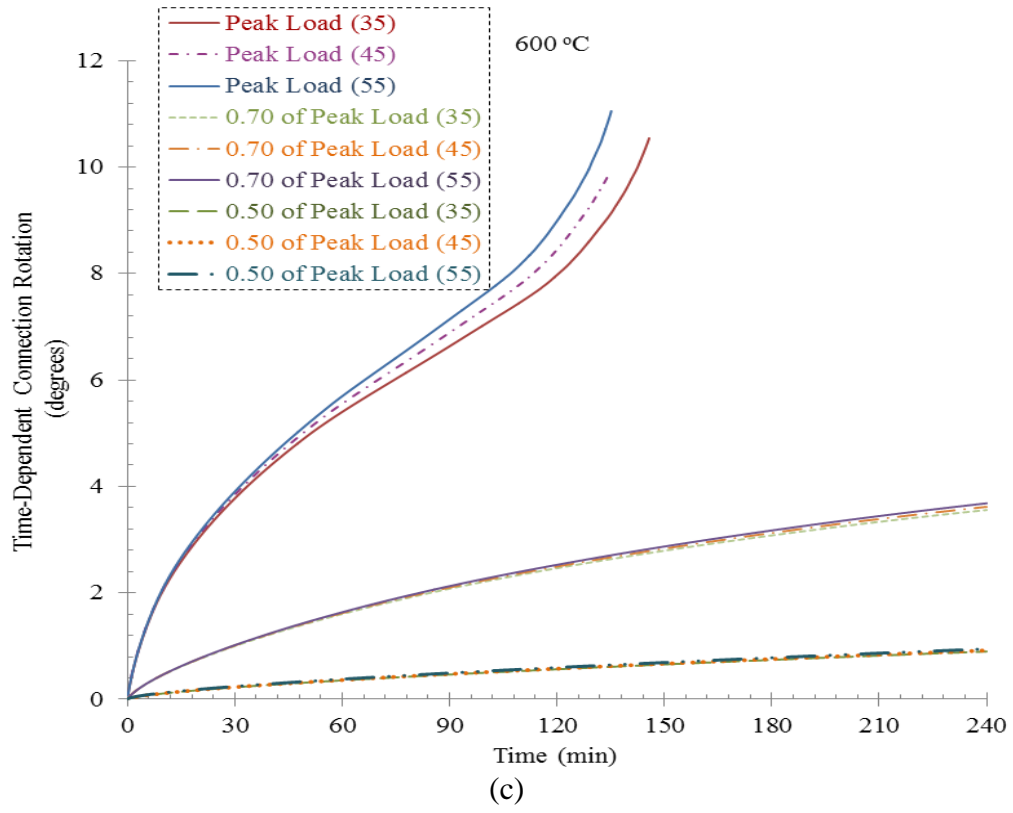
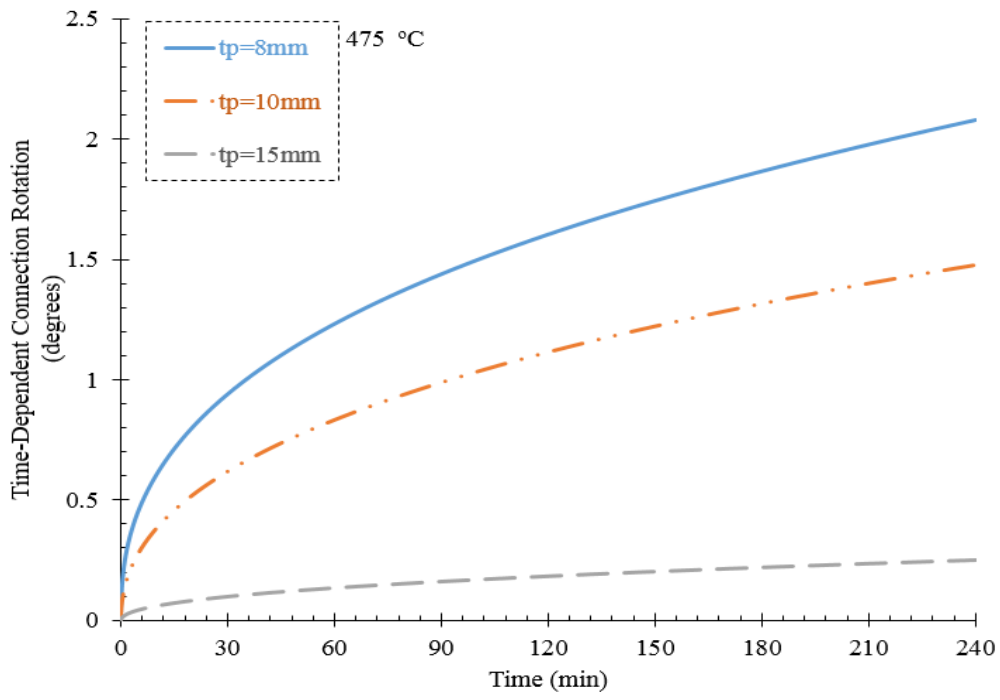
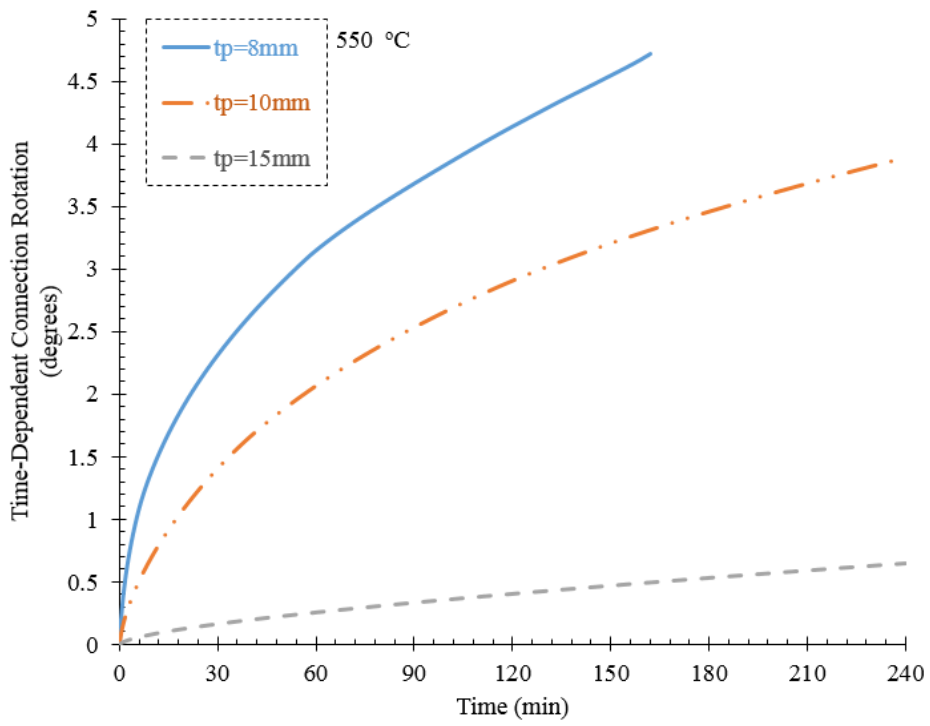


Fig. 18. Effect of Load angle on the time-dependent behavior of flush endplate connection at: (a) 475 °C, (b) 550 °C, (c) 600 °C



(a)



(b)

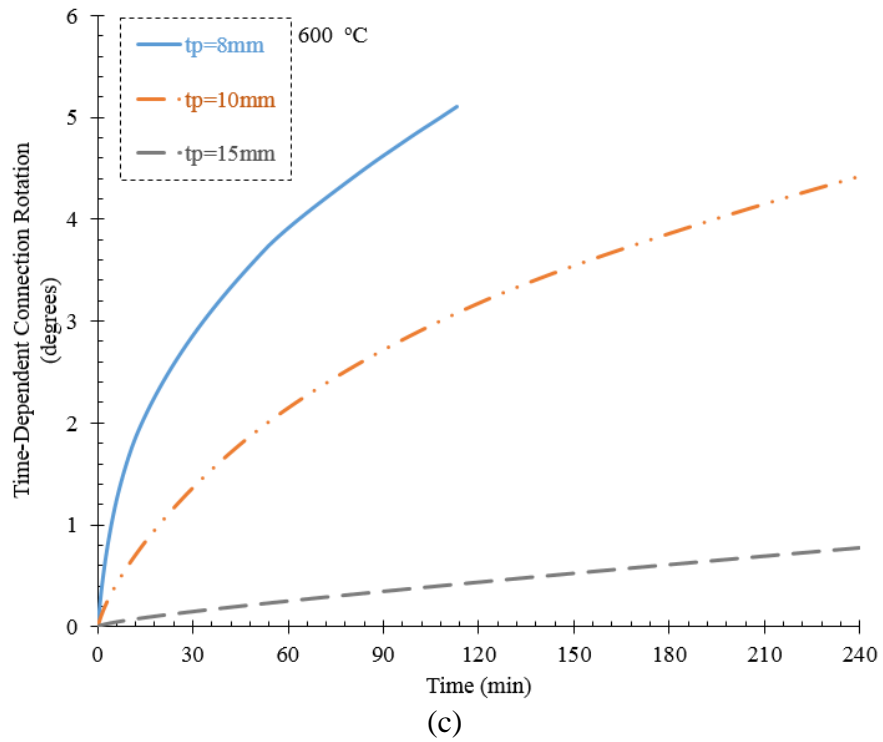
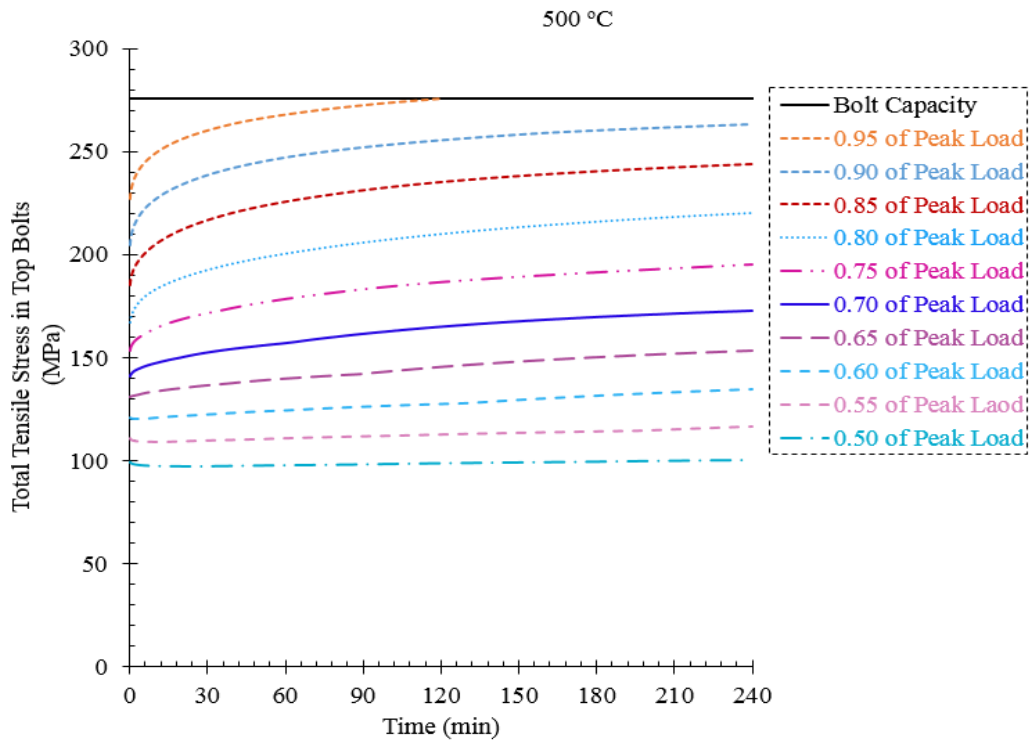
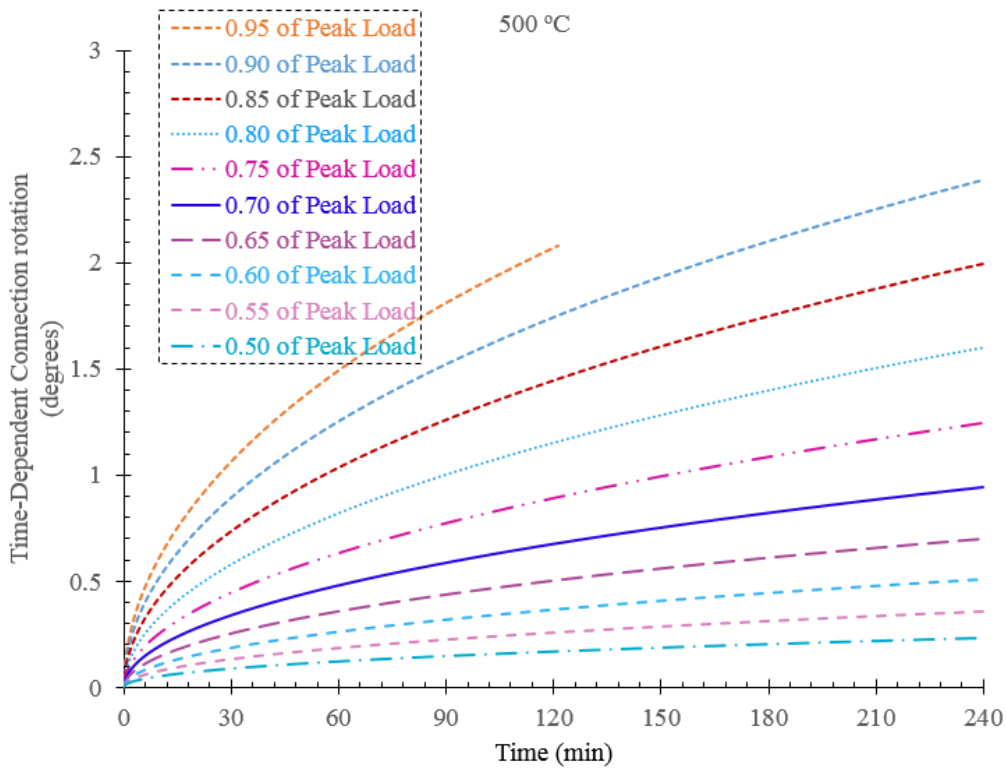


Fig. 19. Effect of endplate thickness on the time-dependent behavior of flush endplate connection at: (a) 475°C, (b) 550 °C, (c) 600 °C

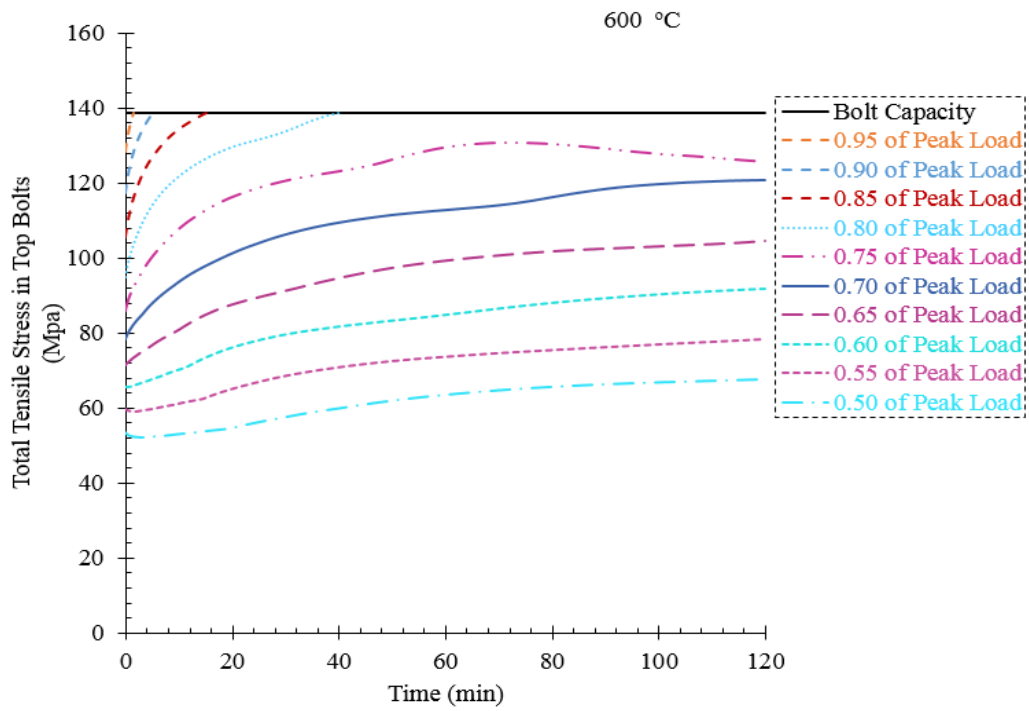


(a)

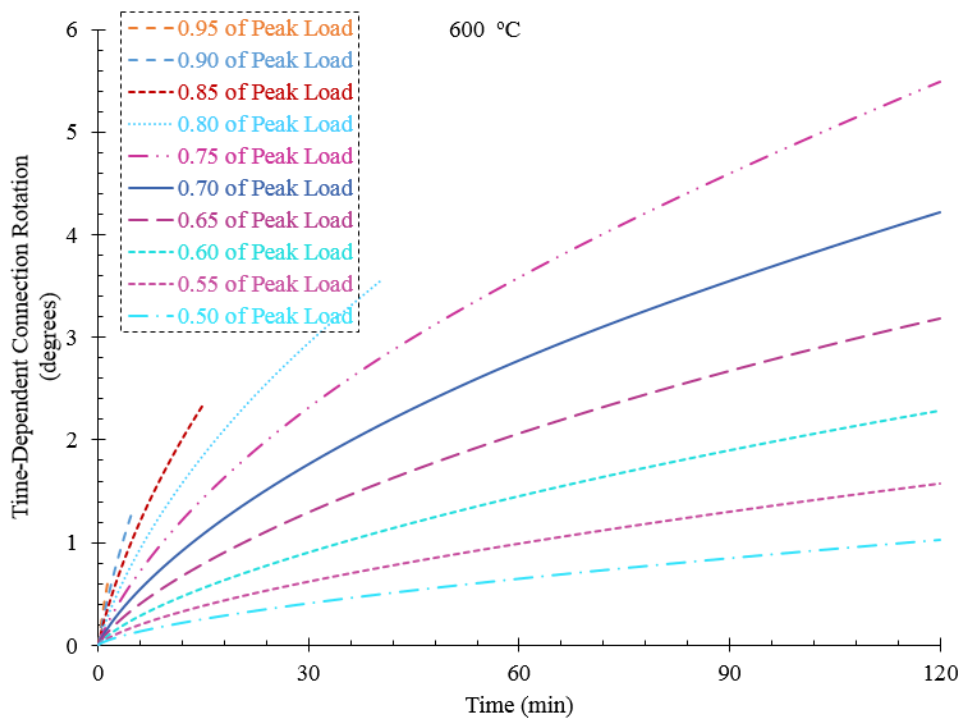


(b)

Fig. 20. Creep behavior of flush endplate connection with M27 bolts at 550 °C: (a) Total tensile stress in top bolts vs. time, (b) Connection rotation vs. time.



(a)



(b)

Fig. 21. Creep behavior of flush endplate connection with M27 bolts at 600 °C: (a) Total tensile stress in top bolts vs. time, (b) Connection rotation vs. time.

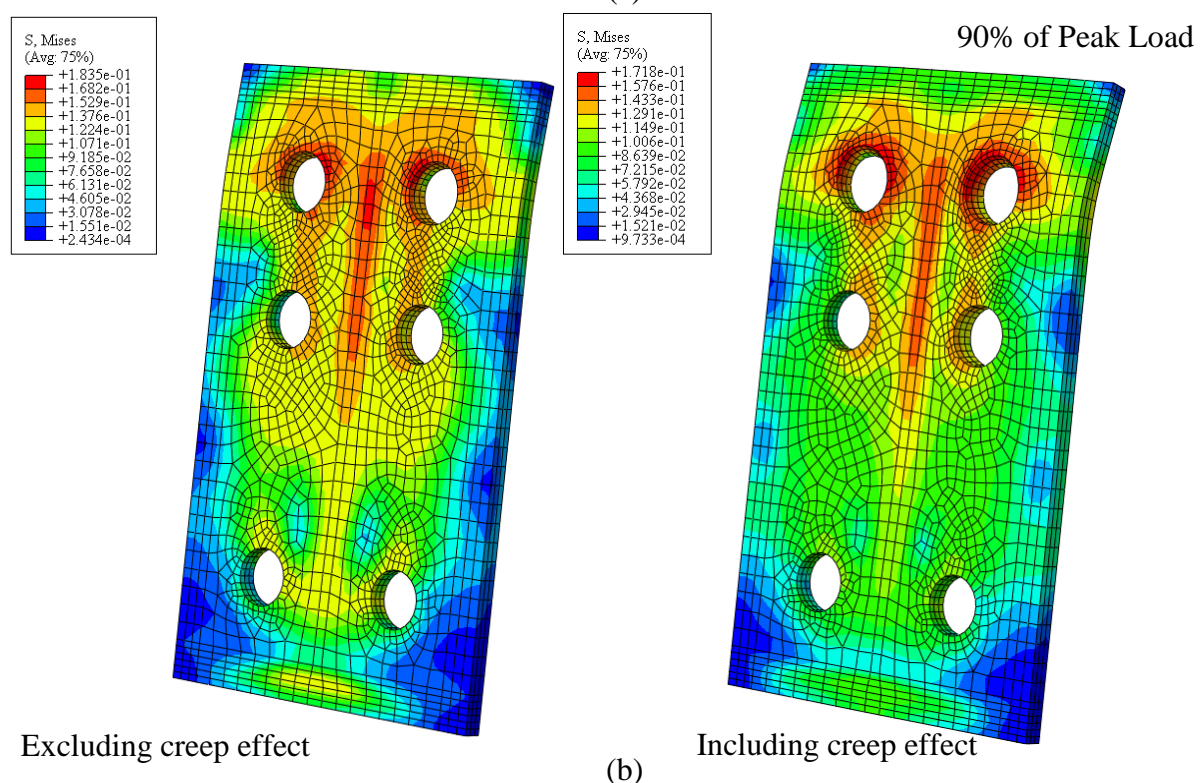
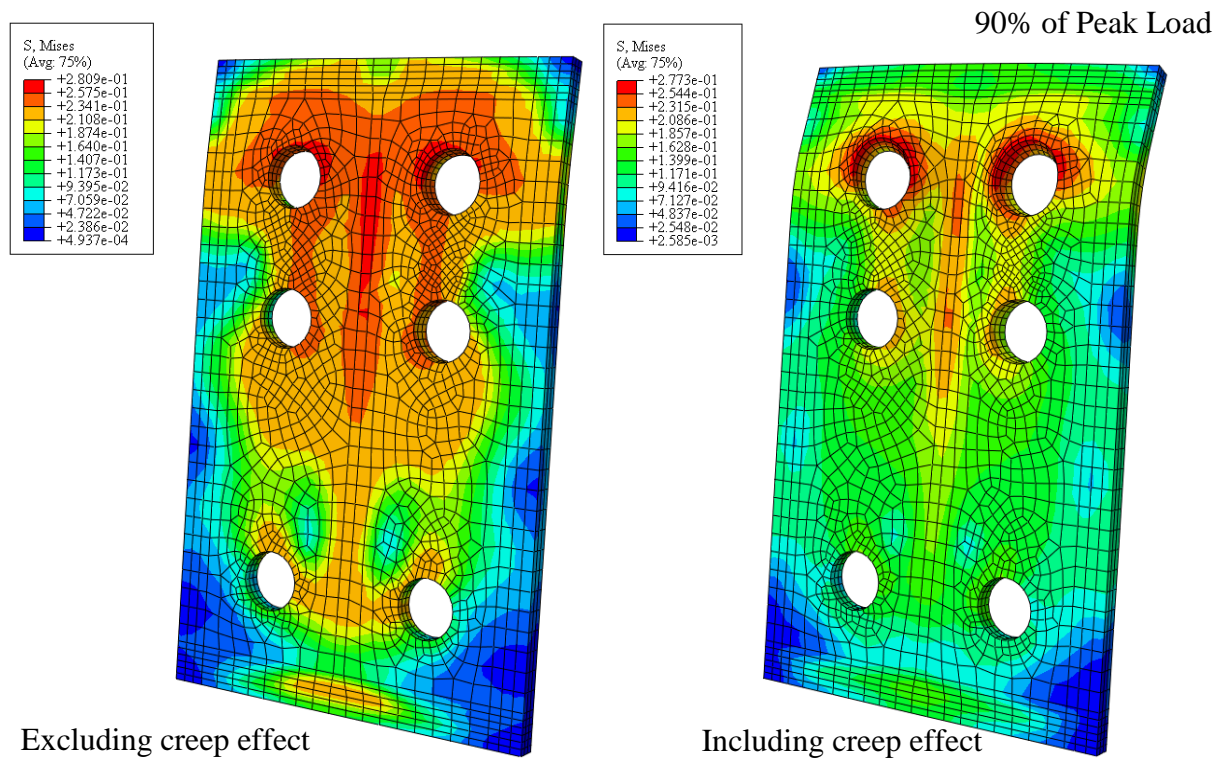
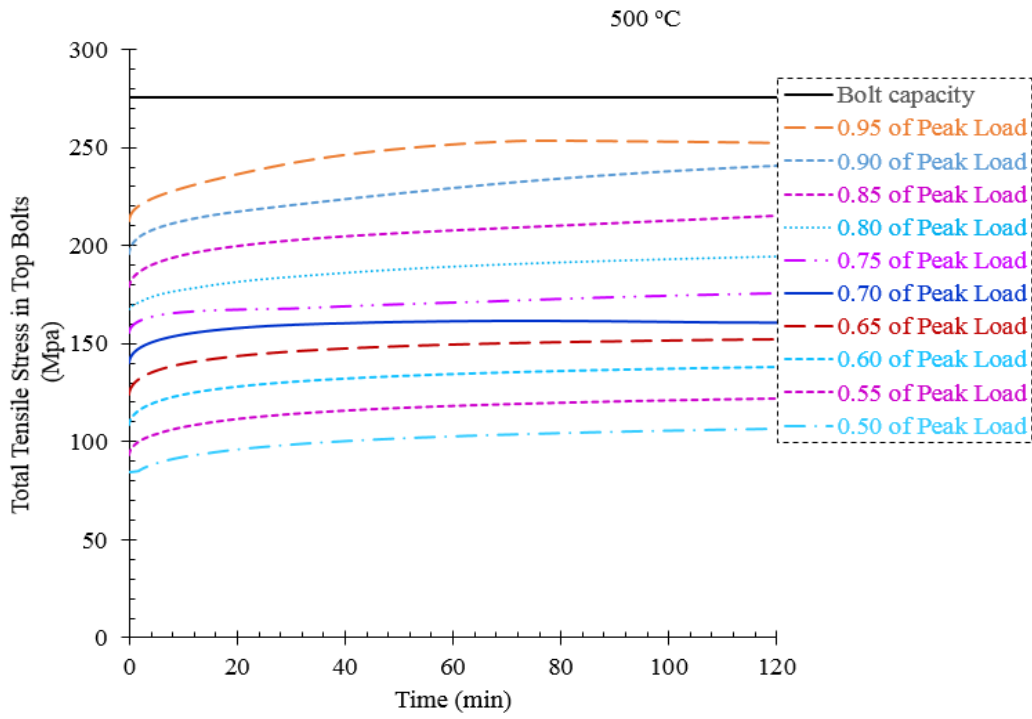
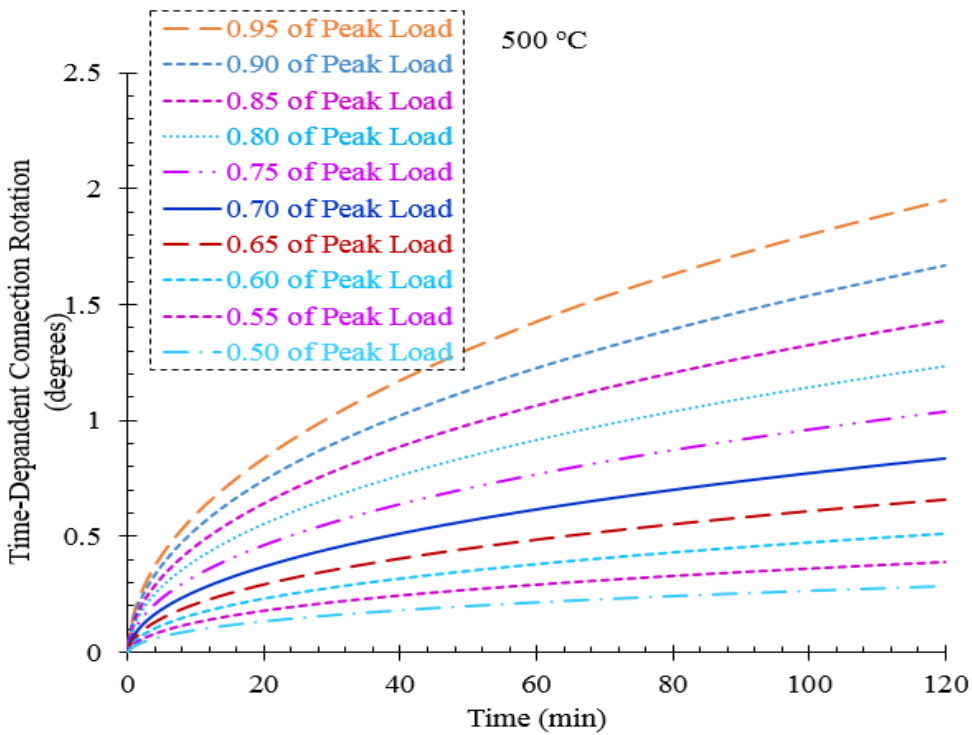


Fig. 22. Stress relaxation in the endplates of test conducted at: (a) 500 °C, (b) 600 °C.



(a)



(b)

Fig. 23. Creep behavior of flush endplate connection with M27 bolts and 8 mm endplate thickness at 500 °C: (a) Total tensile stress in top bolts vs. time, (b) Connection rotation vs. time.

CHAPTER V

MECHANICAL MODELING

A mechanical model is developed to predict the force-connection rotation characteristics of flush endplate connections at elevated temperatures including thermal creep effect. The proposed mechanical model is composed of multi-linear springs that are combined together to predict the rotational stiffness of the whole connection. The multi-linear springs can predict each component stiffness, strength, and rotation capacity. The temperature expressions are based on the ambient temperature formulations proposed in Eurocode3 Part 1.8 (Eurocode3 2005) by considering all material properties as temperature dependent including strength reduction factors (Hu et al. 2007 and Lee et al. 2013). To include the effect of thermal creep in the proposed model, a modified *Burgers* creep model (Findley 1976) is included to model the time-dependent connection rotation of the flush endplate connections when subjected to both constant load and temperature, and it consists of linear springs and viscous dashpots (see Fig. 24).

A. Component stiffness

1. Column web in tension

The column web stiffness, $K_{cw,t}$, acting in tension can be computed as per Eurocode3 and is defined as:

$$K_{cw,t} = \frac{0.7b_{eff,cw,t}t_{cw}}{d_{cw}} E \quad (2)$$

where t_{cw} is the thickness of column web, d_{cw} is the clear depth of column web, $b_{eff,cw,t}$ is the effective width of column web and is assumed to be the effective length of an equivalent T-stub

representing the column flange ($b_{eff,cw,t}$ is the minimum of $[(4m + 1.25e), (2\pi m)]$, and m is the clear distance between the angle fillet and the bolt centerline, and e is the distance between the bolt centerline and the upper edge of the column flange as shown in Fig. 24(a), and E is the modulus of elasticity of the component.

2. Column web in compression

The column web stiffness, $K_{cw,c}$, acting in compression can be computed as per Eurocode3 and is defined as:

$$K_{cw,c} = \frac{0.7b_{eff,cw,c}t_{cw}}{d_{cw}} E \quad (3)$$

where $b_{eff,cw,c}$ is the effective width of column web in compression ($b_{eff,cw,c} = t_{fb} + 2\sqrt{2}a_p + 5(t_{fc} + s) + s_p$, where t_{fb} is beam flange thickness, a_p is the effective weld thickness as shown in Fig. 24(a), and s is equal to the root radius (r_c) for a rolled I or H section column, and s_p is the length obtained by dispersion at 45° through the end-plate and it is taken as endplate thickness t_{ep}).

3. Column web panel in shear

The column web panel in shear stiffness, $K_{cwp,s}$, acting in compression can be computed as per Eurocode3:

$$K_{cwp,s} = \frac{0.38A_{vc}}{\beta z'} E \quad (4)$$

where A_{vc} is the shear area of column web ($A_{vc} = A_c - 2b_c t_{cf} + (t_{cw} + 2r_c)t_{cf}$, where A_c is the cross section area of the column, and b_c is the width of column section, and t_{cf} is the column flange thickness), β is the transformation parameter that is approximately equal to 1 for one sided beam-

column joint, and z' is the lever arm which is approximately equal to the distance between the center of the lower beam flange to the midway between the farthest two bolt rows.

4. Column flange in bending

The flexural stiffness of the column flange, $K_{cf,b}$, is defined as per Eurocode3:

$$K_{cf,b} = \frac{0.9l_{eff,cf,b}^3 t_{cf}^3}{m^3} E \quad (5)$$

where $l_{eff,cf,b}$ is the effective length of column flange defined to be equal to the effective length of equivalent T-stub representing the column flange ($l_{eff,cf,b}$ is the minimum of $[(4m + 1.25e), (2\pi m)]$, more details are shown in Fig. 24(a)).

5. Endplate in bending

The flexural stiffness of the column flange, $K_{ep,b}$, for single row of bolts is defined as per Eurocode3:

$$K_{ep,b} = \frac{0.9l_{eff,ep,b}^3 t_{ep}^3}{m^3} E \quad (6)$$

where $l_{eff,ep,b}$ is the effective length for endplate in tension and is the minimum of $[(4m + 1.25e), (2\pi m)]$ (see Fig. 24(a)).

6. Tension bolts

The tension bolt stiffness, K_{bt} , for single row is defined as per Eurocode3:

$$K_{bt} = \frac{1.6A_b}{L_b} E \quad (7)$$

where A_b is the effective area of the tension bolts, and L_b is the bolt elongation length and is equal to the grip length plus half the sum of the thickness of both bolt head and nut.

B. Equivalent connection stiffness

An equivalent spring stiffness, K_{eq} , can be determined by assembling stiffnesses of the connection components as shown in Fig. 24(b), and is defined as per Eurocode3 and Loster-Jones (1997):

$$K_{eq} = \frac{\sum K_{t,n} h_n}{Z_{eq}} \quad (8)$$

where lever arm h_n available in Eq. (8) can be taken from the center of rotation to the center-line of the bolt row n acting in tension, and n is the bolt row number. $K_{t,n}$ is the equivalent tension zone spring stiffness for a single bolt row at a given temperature and can be expressed using the following equation:

$$\frac{1}{K_{t,n}} = \frac{1}{K_{cw,t}} + \frac{1}{K_{cf,b}} + \frac{1}{K_{ep,b}} + \frac{1}{K_{b,t}} \quad (9)$$

Note that the center of rotation in this analysis was assumed to be the center-line of the lowest bolt row as shown in Fig. 24(b). And Z_{eq} is the equivalent lever arm (see Fig. 24(b)) and is expressed using the following equation as per Eurocode3:

$$Z_{eq} = \frac{\sum K_{t,n} h_n^2}{\sum_n K_{t,n} h_n} \quad (10)$$

C. Determination of rotational stiffness

The rotational stiffness, S_j , of the flush endplate connection can be determined from the stiffnesses of its components, each represented by an elastic stiffness coefficient K_i obtained from the Eurocode3.

The rotational stiffness, S_j , for one bolt row in tension can be calculated as:

$$S_j = \frac{Ez^2}{\mu \sum_i \frac{1}{K_i}} \quad (11)$$

The rotational stiffness, S_j , for multi-bolt row in tension can be calculated as:

$$S_j = \frac{Ez^2}{\mu \sum_i \frac{1}{k_i}} = \frac{Ez^2}{\mu \left(\frac{1}{K_{cw,c}} + \frac{1}{K_{cwp,s}} + \frac{1}{K_{eq}} \right)} \quad (12)$$

where z is the lever arm and is assumed to be taken as Z_{eq} , and μ is the stiffness ratio that is equal to $\frac{S_{j,ini}}{S_j}$, where $S_{j,ini}$ is the initial rotational stiffness of the connection and can be calculated using Eq. (12) for $\mu=1$.

D. Moment and force-rotation curve for flush endplate connection

The moment-rotation characteristics for flush endplate connection can be represented as a tri-linear curve (O-A, A-B, and B-C) representing the elastic, elastic-plastic, and plastic behavior of the connection as shown in Fig. 25. θ_{ld} is the connection rotation at which the applied bending moment, $M_{j,Ed}$, reaches two-third the design moment connection resistance, $M_{j,Rd}$, and it can be written as follows:

$$\theta_{Id} = \frac{2M_{j,Rd}}{3S_{j,ini}} \quad (13)$$

θ_{Xd} is the connection rotation at which $M_{j,Ed}$ reaches $M_{j,Rd}$ and can be written as:

$$\theta_{Xd} = \frac{\lambda M_{j,Rd}}{S_{j,ini}} \quad (14)$$

As per Eurocode3 (2005) and Huang (2011), the stiffness modification coefficient, λ , is equal to 2 for bolted endplate connections. θ_{Cd} is the maximum rotation capacity that the connection can undergo (θ_{Cd} is the connection rotation at which tension top bolt failure or endplate failure occurs). Therefore, the moment-rotation characteristic of flush endplate beam-column connection can be represented as shown in Fig. 25:

$$\text{For } \theta \leq \theta_{Id} \text{ (line OA): } M_{j(\text{segment1})} = S_j \theta = S_{j,ini} \theta \quad (15)$$

$$\text{For } \theta_{Id} < \theta \leq \theta_{Xd} \text{ (line AB): } M_{j(\text{segment2})} = S_j (\theta - \theta_{Id}) + \frac{2}{3} M_{j,Rd} \quad (16)$$

$$\text{For } S_j = \frac{M_{j,Rd}}{3(\theta_{Xd} - \theta_{Id})}$$

$$\text{For } \theta_{Xd} < \theta \leq \theta_{Cd} \text{ (line BC): } M_{j(\text{segment3})} = S_j (\theta - \theta_{Xd}) + M_{j,Rd} \quad (17)$$

$$\text{For } S_j = 0.001208 S_{j,ini} \text{ for } T = 20 \text{ } ^\circ C$$

$$S_j = 0.001208 \left(\frac{f_{yT}}{f_{uT}} \right)_F S_{j,ini} \text{ for } T \geq 450 \text{ } ^\circ C$$

The ratio $\left(\frac{f_{yT}}{f_{uT}} \right)_F$ is the yield strength to tensile strength ratio for the connection component

that governs the behavior of the connection.

E. Connection resistance

1. Moment resistance, $M_{j,Rd}$:

The moment resistance, $M_{j,Rd}$, for a beam-column connection can be calculated as the minimum of $M'_{j,Rd}$ and $M''_{j,Rd}$ and they can be defined respectively, as follows:

$$M'_{j,Rd} = \frac{F_{b,max} I_b}{A_b (y_n - x)} \left(\frac{f_{y,b}}{f_{u,b}} \right) \quad (18)$$

$$M''_{j,Rd} = \sum_n h_n F_{tr,Rd} \quad (19)$$

where, $F_{b,max}$ is the maximum load applied on the top bolts due to combined shear and tension forces applied on the connection, $\left(\frac{F_{b,max}}{A_b} = (1.3(f_{nt}) - \left(\frac{f_{nt}}{f_{nv}} \right) f_v) \right)$ where f_{nt} , f_{nv} , f_v are nominal tensile strength of the bolt, nominal shear strength of the bolt, and required shear stress due to applied load, respectively), I_b is the moment of inertia for the bolt group, y_n is the distance from the bottom of the endplate to the center-line of each bolt row, x is the distance from the bottom of the endplate to the neutral axis of the bolt group, and $\frac{f_{y,b}}{f_{u,b}}$ is a ratio used to account for strain hardening of the bolt material, $F_{tr,Rd}$ is the effective design tension resistance of bolt row n and must be calculated for each bolt row in sequence starting from the farthest bolt row in tension with respect to the center of rotation.

The effective tension resistance $F_{tr,Rd}$ for a single bolt row must be taken as the smallest value of the resistance of column flange in bending, column web in tension, endplate in bending, and beam web in tension.

2. Column flange in bending, $F_{t,cf,Rd}$:

The tension resistance, $F_{t,cf,Rd}$, of column flange in bending is obtained by assuming the column flange to act as an equivalent T-stub of length $l_{eff,cf,b}$ (Leston-Jones 1997; Eurocode3 2005), and is written as follows:

$$F_{t,cf,Rd} = \frac{4M_{pl,fc}}{m} \quad (20)$$

where $M_{pl,fc}$ is the plastic moment capacity of an equivalent T-stub and is equal to $0.25l_{eff,cf,b}t_{cf}^2f_{yt,cf}$ (where $f_{yt,cf}$ is the yield strength of the column flange at given temperature).

3. Column web in tension, $F_{t,cw,Rd}$:

The design resistance, $F_{t,cw,Rd}$, of an unstiffened column web subject to transverse tension can be determined as per Eurocode3:

$$F_{t,cw,Rd} = \frac{\omega b_{eff,cw,t} t_{cw} f_{yt,cw}}{\gamma_{Mo}} \quad (21)$$

where ω is a reduction factor to allow for the interaction with shear in the column web panel and can be calculated a $\omega = \frac{1}{\sqrt{1+1.3(b_{eff,cw,t} t_{cw} / A_{vc})^2}}$ for β equals to 1. $f_{yt,cw}$ is the yield strength of the column web at given temperature, and γ_{Mo} is partial factor for resistance of cross section and is equal to 1 for buildings.

4. Endplate in bending, $F_{t,ep,Rd}$:

The tension resistance $F_{t,ep,Rd}$ of endplate in bending can be estimated by assuming the endplate to act as an equivalent T-stub of length $l_{eff,ep,b}$ (Leston-Jones 1997; Eurocode3 2005)

$$F_{t,ep,Rd} = \frac{4M_{pl,ep}}{m} \quad (22)$$

where $M_{pl,ep}$ is the plastic moment capacity of an equivalent T-stub and is equal to $0.25l_{eff,ep}t_{ep}^2f_{yt,ep}$, $f_{yt,ep}$ is the yield strength of the endplate at given temperature.

5. Beam web in tension, $F_{t,bw,Rd}$:

The tension resistance $F_{t,bw,Rd}$ of beam web in tension can be estimated as per Eurocode3:

$$F_{t,bw,Rd} = \frac{b_{eff,bw,t}t_{bw}f_{yt,bw}}{\gamma_{Mo}} \quad (23)$$

where $b_{eff,bw,t}$ of the beam web in tension should be taken as equal to the effective length of the equivalent T-stub representing the endplate in bending ($b_{eff,bw,t} = l_{eff,ep}$), $f_{yt,bw}$ is the yield strength of the beam web at given temperature, and t_{wb} is the thickness of the beam web.

6. The maximum bending moment of the connection, M_{Cd} :

M_{Cd} is defined as the maximum applied moment at failure of the connection. The two potential failure modes of flush endplate connection is governed by either top tension bolt failure or endplate failure. Thus, M_{Cd} can be estimated as the minimum of $M'_{j,Rd} \left(\frac{f_{ut,b}}{f_{yt,b}} \right)$ and $M''_{j,Rd} \left(\frac{f_{ut,ep}}{f_{yt,ep}} \right)$,

where $\frac{f_{ut,b}}{f_{yt,b}}$ and $\frac{f_{ut,ep}}{f_{yt,ep}}$ are ratios used to estimate the maximum moment for both top bolts and endplate failure, respectively.

F. Inclusion of thermal creep in the mechanical model

A modified *Burgers* model is used to model the effect of thermal creep of flush endplate connections in fire. The *Burgers* model was modified by using creep connection rotation instead of creep strain. This assumption is based on the direct relationship between the creep connection

rotation and the creep strain. The modified *Burgers* model consists of a combination of *Maxwell* model and *Kelvin-Voight* model in series as shown in Figs. 26 (Findley 1976). The *Maxwell* model consists of a linear spring K_1 and a viscous dashpot η_1 connected in series. The linear spring K_1 represents the equivalent stiffness of the connection components in tension connected in series with shear column web stiffness and compression column web stiffness as shown in Fig. 26. The viscous dashpot η_1 represents the secondary stage of the time-dependent creep curve as shown in Fig. 27(a). *Kelvin-Voight* model consists of elastic spring K_2 and viscous dashpot η_2 that are connected in parallel to represent the primary stage of typical time-dependent creep curve as shown in Fig. 27(b) (Findley 1976). Figure 27(c) represents the time-dependent connection rotation (modified *Burgers* model) used in this study.

1. Modified Burgers model

The total connection rotation (r) under constant stress σ_0 at time t is the summation of the rotations resulting from *Maxwell* model (θ, r_1) and *Kelvin-Voight* model (r_2) as shown in Fig. 26:

$$r = \theta + r_1 + r_2 \quad (24)$$

where θ is time-independent connection rotation and is resulting from the steady-state temperature analysis and can be written in function of K_1 as follows:

$$\theta = \frac{\sigma_0}{K_1} \quad (25)$$

r_1 is the time-dependent rotation resulting from dashpot η_1 :

$$r_1 = \frac{\sigma_0 t}{\eta_1} \quad (26)$$

Since linear spring K_1 , and viscous dashpot η_1 are connected in series forming a *Maxwell* model as shown in Fig. 26, the total rotation of *Maxwell* model, r_M , under constant stress σ_0 can be written as a function of time, t :

$$r_M(t) = \frac{\sigma_0}{K_1} + \frac{\sigma_0}{\eta_1} t \quad (27)$$

r_2 is the time-dependent connection rotation resulting from the *Kelvin-Voight* model and can be calculated using the following 1st order equation:

$$\dot{r}_2 + \frac{K_2}{\eta_2} r_2 = \frac{\sigma_0}{\eta_2} \quad (28)$$

where \dot{r}_2 is the connection rotation rate and the corresponding solution of Eq. (28) under a constant stress σ_0 applied is:

$$r_2(t) = \frac{\sigma_0}{K_2} (1 - e^{-\frac{K_2}{\eta_2} t}) \quad (29)$$

Therefore the modified *Burgers* model equation used to predict the total connection-rotation characteristics can be written as follows:

$$r(t) = \theta + \frac{\sigma_0}{\eta_1} t + \frac{\sigma_0}{K_2} (1 - e^{-\frac{K_2}{\eta_2} t}) \quad (30)$$

The results of the FE time-dependent connection rotation characteristics at different elevated temperatures with different loads to peak load ratios are used to compute the constants available in the modified *Burgers* equation ($\eta_1, \eta_2, \text{and } K_2$) Eq.(30). In order to get these constants, the modified *Burgers* equation is divided into two parts. The first part is the time-dependent connection rotation $\frac{\sigma_0}{\eta_1} t$ which represents the *Maxwell-dashpot* in the modified

Burgers model. This part represents the secondary stage of a typical creep curve where creep rotation is almost linear with respect to time as shown in Fig. 27(a). The second part is the time-

dependent connection rotation that is equal to $\frac{\sigma_0}{K_2}(1 - e^{-\frac{K_2 t}{\eta_2}})$. This part is the solution of Kelvin-

Voigt model in the modified *Burgers* model and represents the primary stage of a typical creep curve where the curve is non-linear and exhibits a decreasing creep rotation rate as shown in Fig.

27(b). The constants $\frac{\sigma_0}{K_2}$ and $\frac{K_2}{\eta_2}$ in Eq. (28) can be calculated using *Euler* integration method.

Euler integration method is a numerical procedure used to solve ordinary differential equation with a given initial value and small time increments for integration (Torić and Burgess 2016). $\frac{\sigma_0}{\eta_1}, \frac{\sigma_0}{K_2}$

, and $\frac{K_2}{\eta_2}$ available in Eq. (30) at different elevated temperatures for different applied loads can be

calculated as follows:

$$\frac{\sigma_0}{\eta_1} = c_1 \frac{l_a}{P} - c_2 \quad (31)$$

$$\frac{\sigma_0}{K_2} = c_3 e^{c_4 \frac{l_a}{P}} \quad (32)$$

$$\frac{K_2}{\eta_2} = \frac{\frac{\sigma_0}{\eta_2}}{\frac{\sigma_0}{K_2}} \quad (33)$$

$$\frac{\sigma_0}{\eta_2} = c_5 e^{c_6 \frac{l_a}{P}} \quad (34)$$

where T is temperature in ($^{\circ}\text{C}$), l_a is the applied load in (kN), P is the peak load that the connection can withstand at any temperature in (kN) (note that $\frac{l_a}{P}$ ratio is in percent), and c_1, c_2, c_3, c_4, c_5 , and c_6 are constants, and they are tabulated in Table 1.

2. Maximum connection rotation prediction

When including the thermal creep material in the beam and the endplate, the thermal creep tends to relax the beam by increasing its deflection. This increase in deflection generates higher catenary forces in the connection. Thus, as connection rotation increases due to thermal creep effects, an induced tensile stress developed in the top bolts of the flush endplate connection leading to tension bolt failure. Using FE simulations conducted on thermal creep behavior of flush endplate connections, the maximum time-dependent connection rotation that the connection can withstand:

$$\theta_{(\%P)}^t = \theta_{(\%P)_{Total}} - \theta_{\%P} \quad (35)$$

where is $\theta_{(\%P)_{Total}}$ is the maximum connection rotation that the connection can withstand including thermal creep effect at any load to peak load ratio ($\theta_{(\%P)_{Total}} = (a(\frac{l_a}{P})^2 - b\frac{l_a}{P} + c)\theta_p$), where θ_p is the maximum connection rotation that the connection can resist under steady-state temperature analysis, a, b , and c are constants and are available in Table 3 and are only used for flush endplate connections having geometric properties illustrated in Fig. 24, and $\theta_{\%P}$ is the connection rotation that the connection can undergo at any given load to peak load ratio excluding thermal creep effect. Note that θ_p and $\theta_{\%P}$ can be estimated using the proposed mechanical model when thermal creep effect is neglected.

3. Effect of different geometrical parameters on the time-dependent behavior of flush endplate connections in fire

A model that uses geometric and mechanical properties is able to predict the time-dependent behavior of flush endplate connections in fire. After identifying the major parameters that impact the total connection rotation (r) which was found to be the bolt diameter and the endplate thickness, two dimensionless factors α and γ are multiplied by Eq. (30) to account for different bolt diameter and different plate thickness, respectively and can be written as follows:

$$r(t) = \theta + \left(\frac{\sigma_0 t}{\eta_1} + \frac{\sigma_0}{K_2} (1 - e^{-\frac{K_2 t}{\eta_2}}) \right) \alpha \gamma \quad (36)$$

where α is a bolt diameter dimensionless factor and is equal to $\left(\frac{P d_b 100}{d_{M20} l_a} \right)$, γ is a plate thickness dimensionless factor and is equal to $\left(\frac{P t_{ep} 100}{t_{10} l_a} \right)$, d_b is bolt diameter, d_{M20} is the M20 bolt diameter, and t_{10} is the 10 mm plate thickness. Also, α and γ are dependent on the applied load to peak load ratio to account for the influence of different load ratios on the thermal creep behavior of flush endplate connections having different geometrical properties. Note that α and γ are equal to 1 for M20 bolts and 10 mm plate thickness, respectively. Note that Eq. (36) is an approximate estimation of the connection rotation that can be used for large load to peak load ratios.

G. Proposed model performance

A comparison of the proposed mechanical model with FE results of the flush endplate connections with and without thermal creep effect is presented. Figures 28(a) and 28(b) show that the proposed mechanical model can predict with reasonable accuracy the time-independent FE

total force-rotation resistance response as far as strength, stiffness, and ductility at ambient and elevated temperatures. Also, the proposed mechanical model can predict with good agreement the time-dependent connection rotation at elevated temperatures (from 450 °C to 600 °C) as shown in Figs. 29 and 30. Further, the mechanical model is able to predict the failure modes resulted from both steady-state temperature analysis and steady-state creep analysis. More specifically, in the steady-state temperature analysis, both the FE simulations and proposed mechanical model show that endplate failure occurs at temperatures smaller than or equal to 450 °C and tension top bolt failure occurs at temperatures larger than 450 °C. Whereas for temperature ranging from 450 °C to 600 °C with 25 °C increment, both FE simulations and proposed mechanical model show that tension bolt failure governs the connection behavior. Noted that the mechanical model is able to predict the thermal creep behavior of the flush endplate connection at any given load to peak load ratio larger than 50%.

Furthermore, steady-state temperature creep analysis is used to develop a transient creep analysis by producing isochronous rotation-temperature curves to evaluate the effect of thermal creep on the performance of flush endplate connection in a fire event. A representative of these isochronous rotation-temperature curves for a constant load of 76 kN is shown in Fig. 31. Where 76 kN represents the peak load resulted from the steady-state temperature analysis at 600 °C. It can be seen that the mechanical model can predict with high accuracy the isochronous rotation-temperature curves that represents the response of the connection under a real fire (transient analysis). The results show that the approximate method predict with good accuracy the time-dependent behavior of flush endplate connection having different geometrical parameters especially for high load to peak load ratios (see Fig. 32).

Table 2. Constants used in modified *Burgers* model equation.

Temperature (°C)	c_1	c_2	c_3	c_4	c_5	c_6
450	0.000090	0.0042	0.0078	0.0513	0.0007	0.0524
475 ¹	0.000100	0.0051	0.0044	0.0549	0.0004	0.0541
500 ²	0.000116	0.0060	0.0034	0.0565	0.0003	0.0547
525 ²	0.000195	0.0096	0.0050	0.0596	0.0004	0.0559
550	0.000290	0.0137	0.0089	0.0590	0.0007	0.0558
575 ²	0.000400	0.0171	0.0085	0.0632	0.0006	0.0590
600	0.000536	0.0260	0.0108	0.0644	0.0007	0.0607
Exceptions: 1: c_1 is slightly modified for 50% and 55% peak load ratio and is equal to 1.09E-04. 2: c_1 is slightly modified for 50% and is equal to 1.2E-04, 2E-04, and 3.7E-04 for 500 °C, 525 °C, 575 °C.						

Table 3. Constants used in estimating the maximum connection rotation.

Temperature (°C)	a	b	c
450	0	0.0107	2.68470
475	0.00020	0.0526	4.36740
500	0.00081	0.1663	9.52700
525	0.00081	0.1663	9.52700
550	0.00066	0.1334	7.72900
575	0.00110	0.2119	11.1989
600	0.00060	0.1215	7.24220

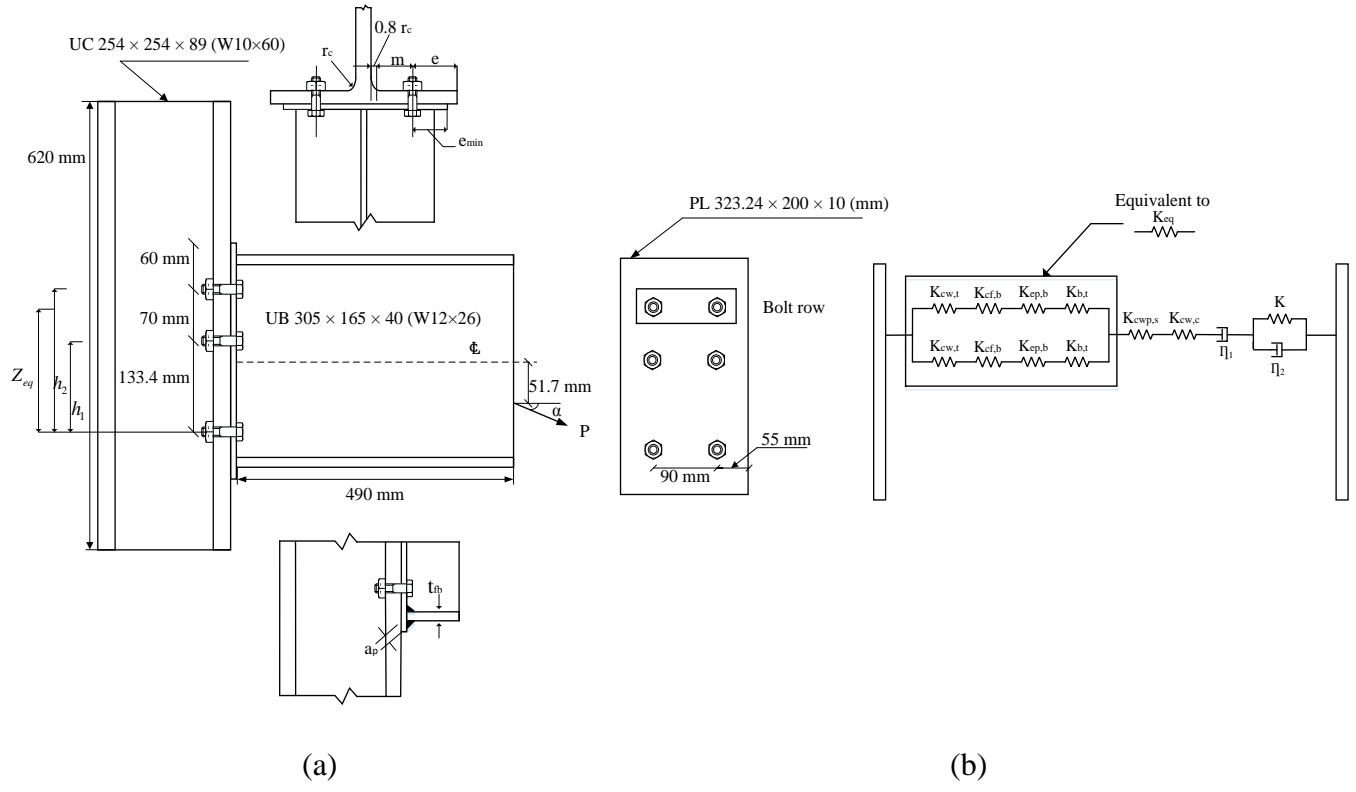


Fig. 24. Flush endplate connection configuration utilized in the study: (a) geometrical properties, (b) component stiffnesses assembly including dashpots.

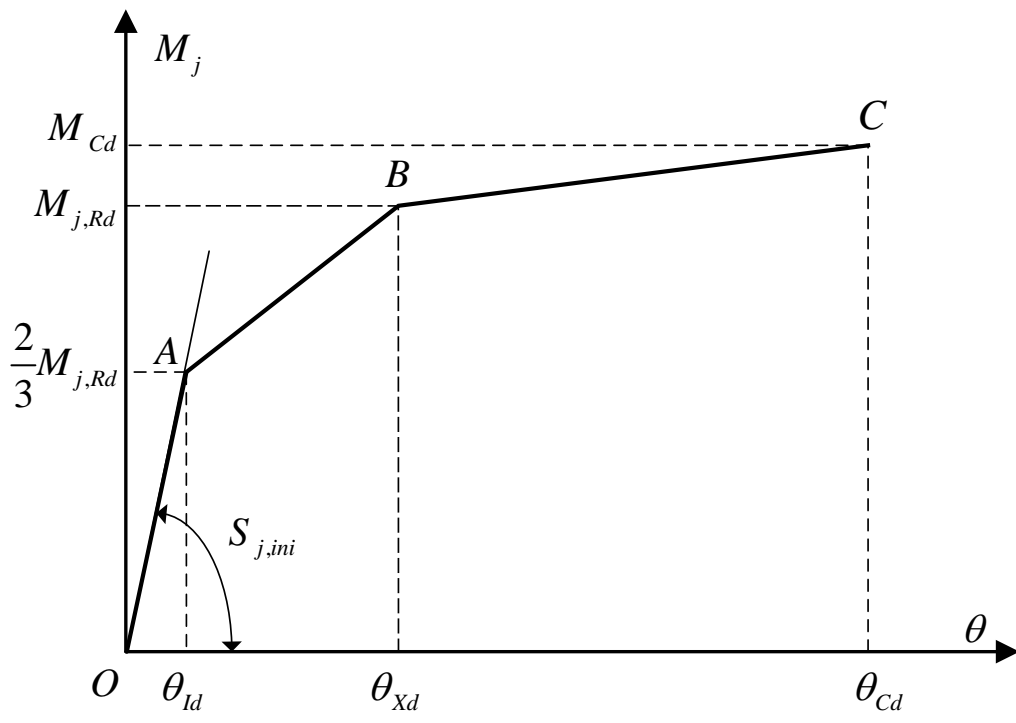


Fig. 25. Tri-linear moment-rotation characteristic.

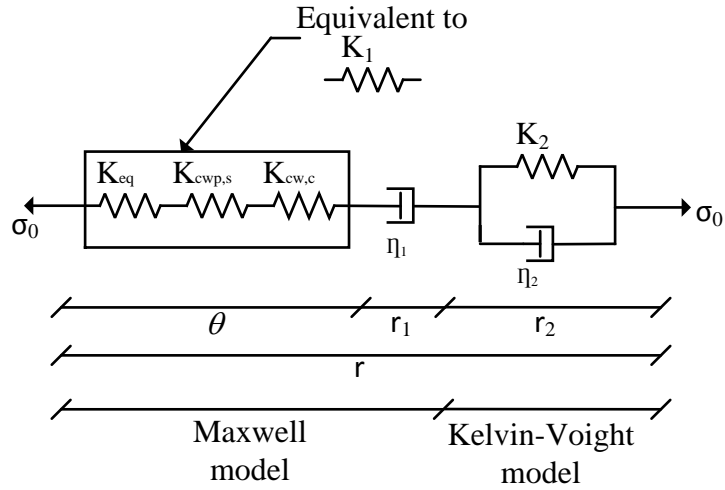


Fig. 26. Modified *Burgers* model.

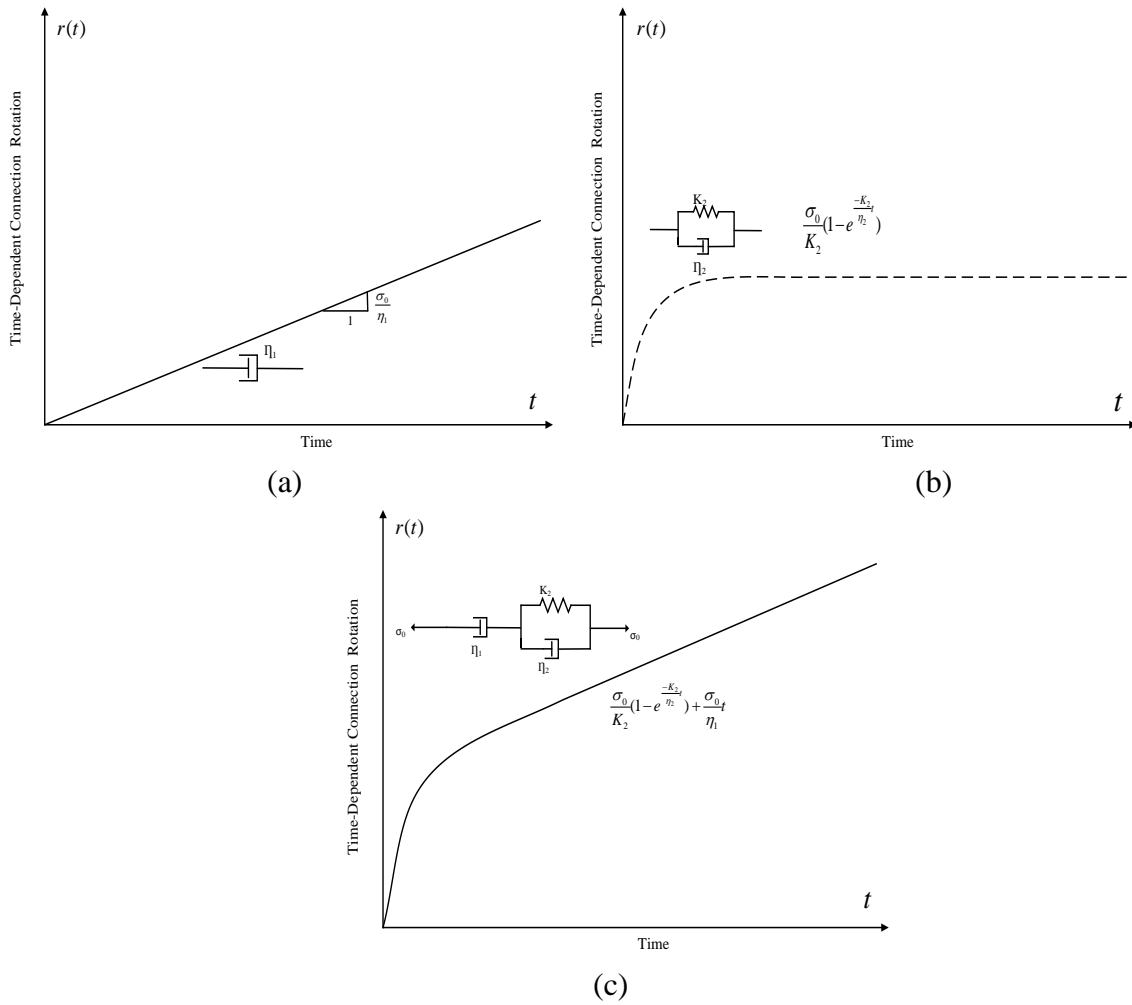
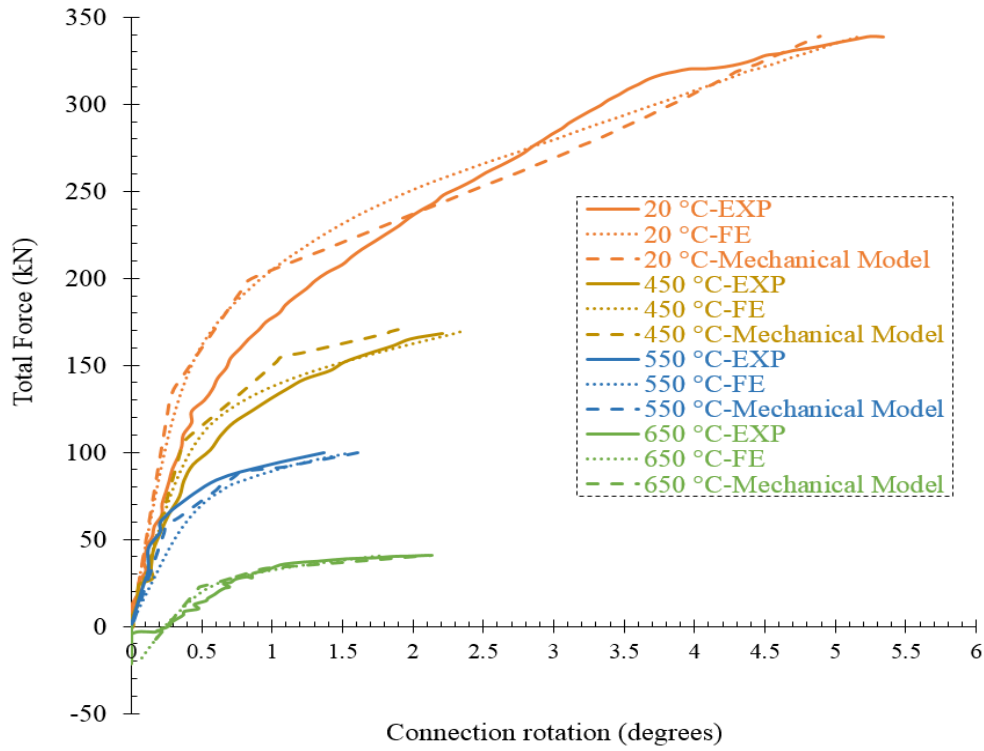
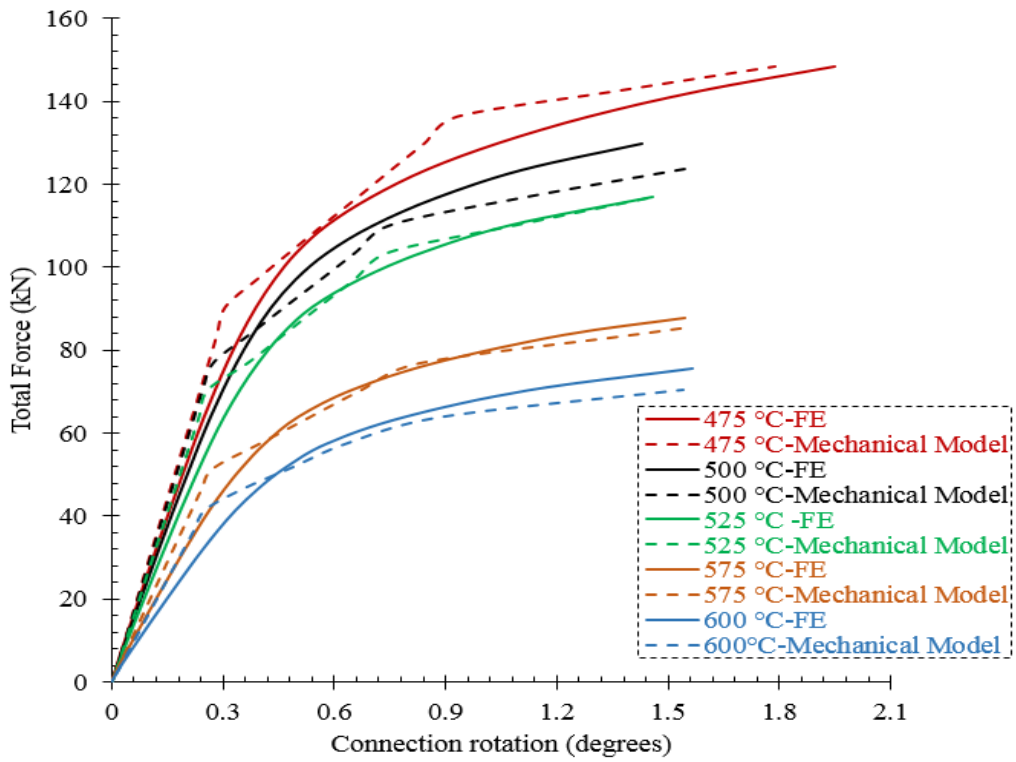


Fig. 27. Time-dependent connection behavior: (a) Maxwell dashpot, (b) *Kelvin-Voigt* model, (c) modified *Burgers* model.

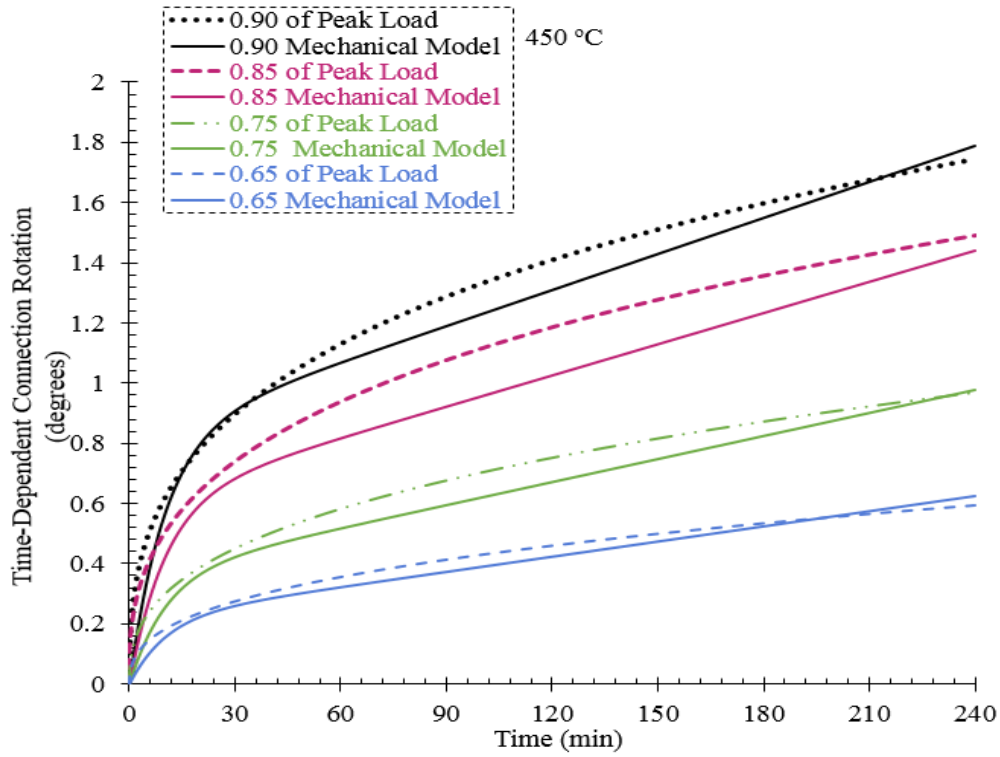


(a)

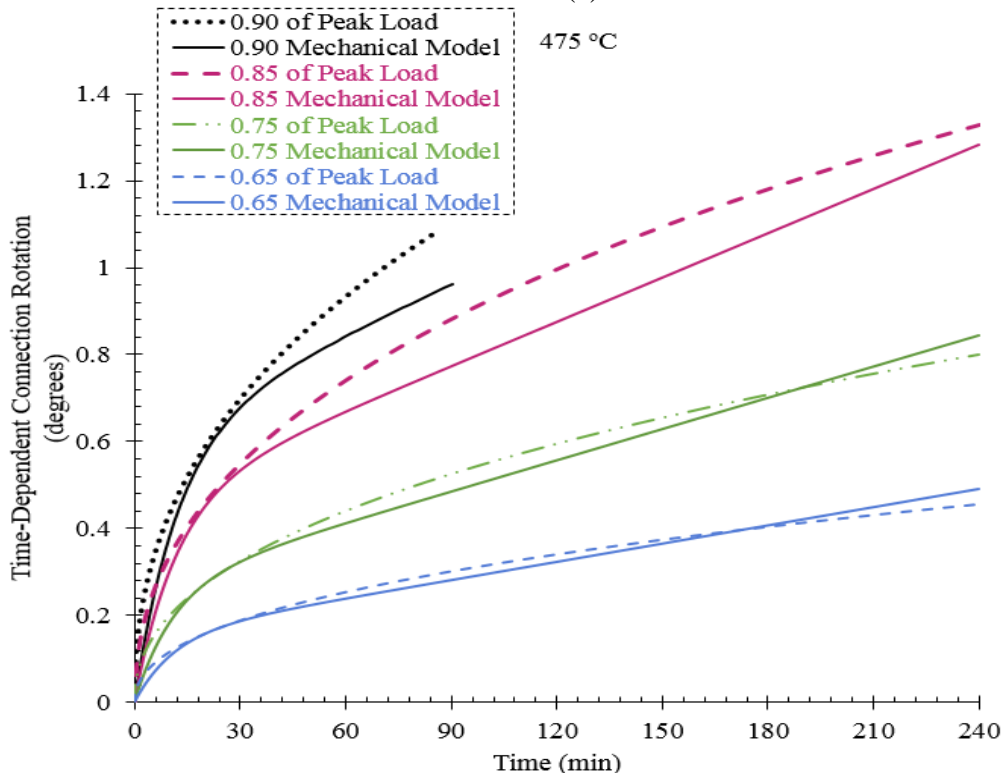


(b)

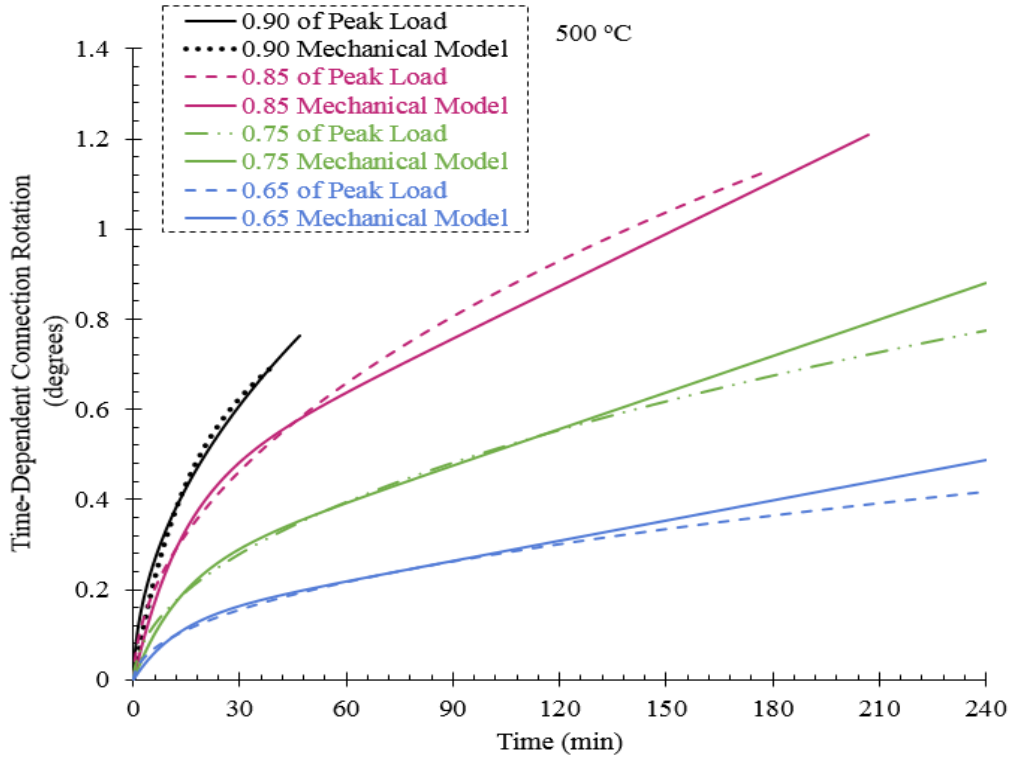
Fig. 28. Time-independent behavior of flush endplate connection: (a) Experimental vs. FE vs. mechanical model predictions, (b) FE vs. mechanical model predictions.



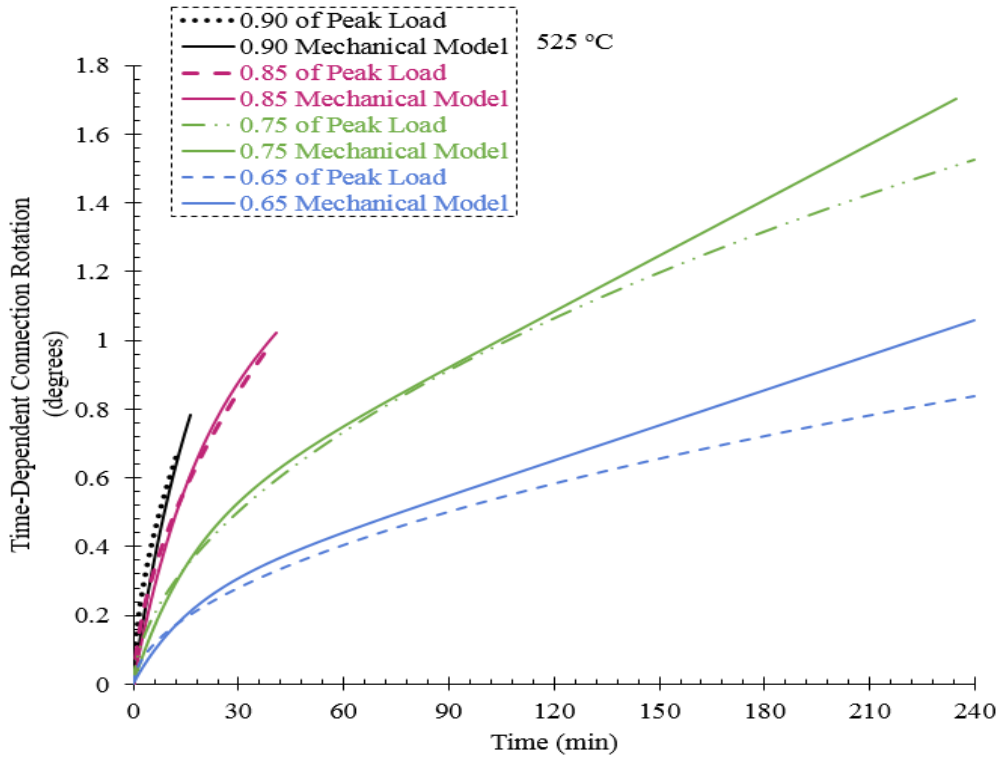
(a)



(b)

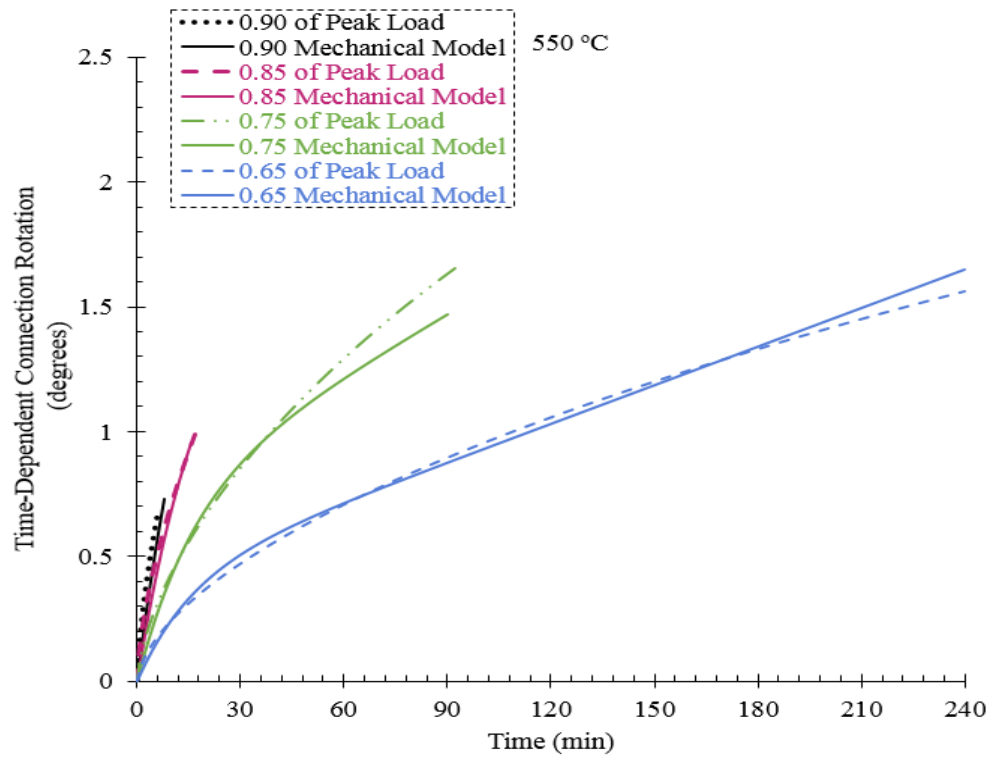


(c)

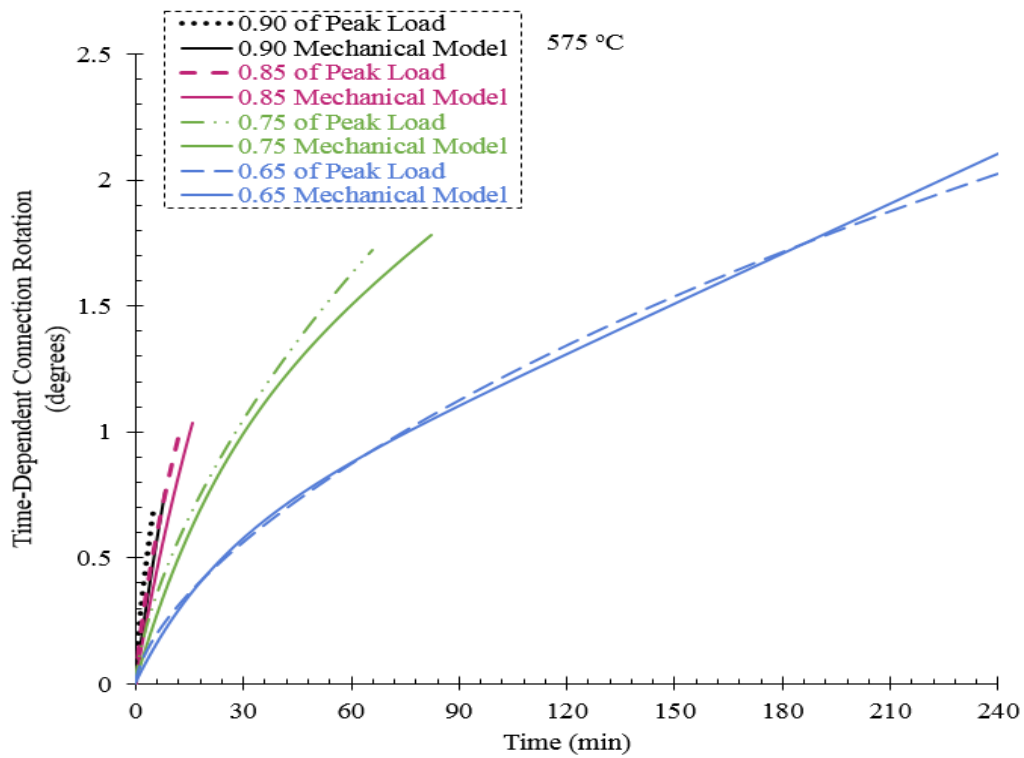


(d)

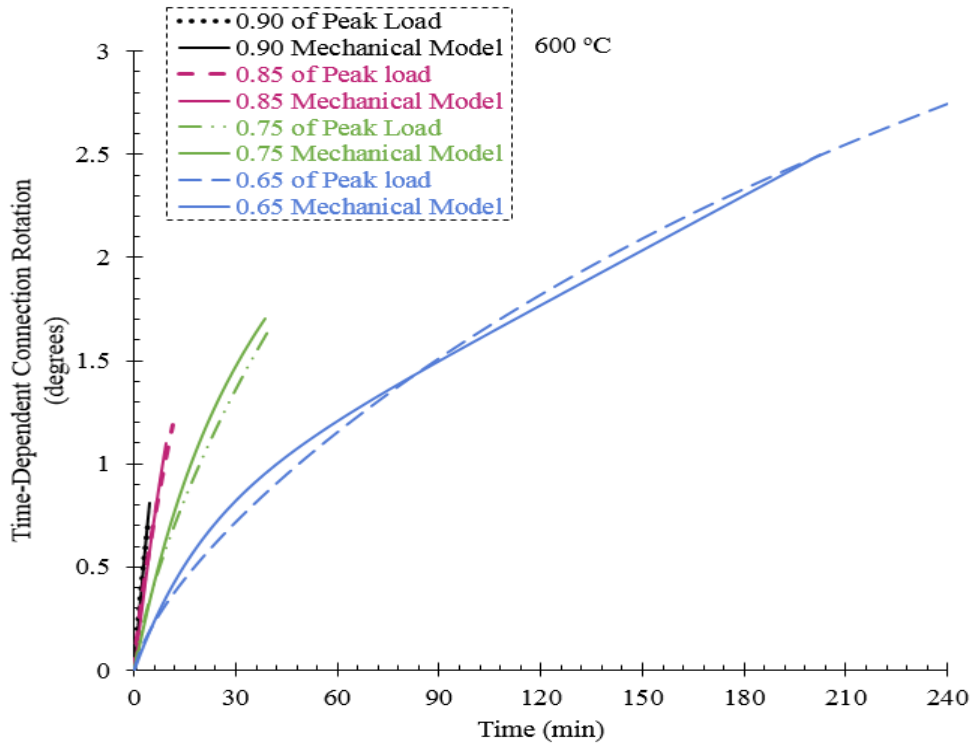
Fig. 29. FE vs. mechanical model of flush endplate connection behavior at: (a) 450 °C, (b) 475 °C, (c) 500 °C, (d) 525 °C.



(a)



(b)



(c)

Fig. 30. FE vs. mechanical model of flush endplate connection behavior at: (a) 550 °C, (b) 575 °C, (c) 600 °C.

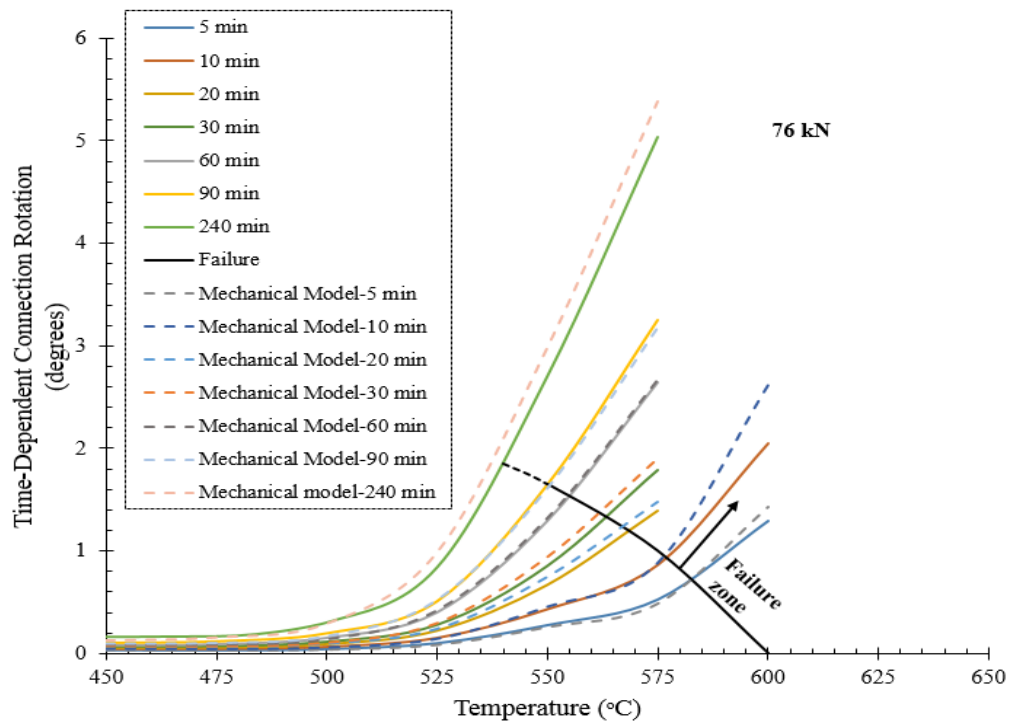
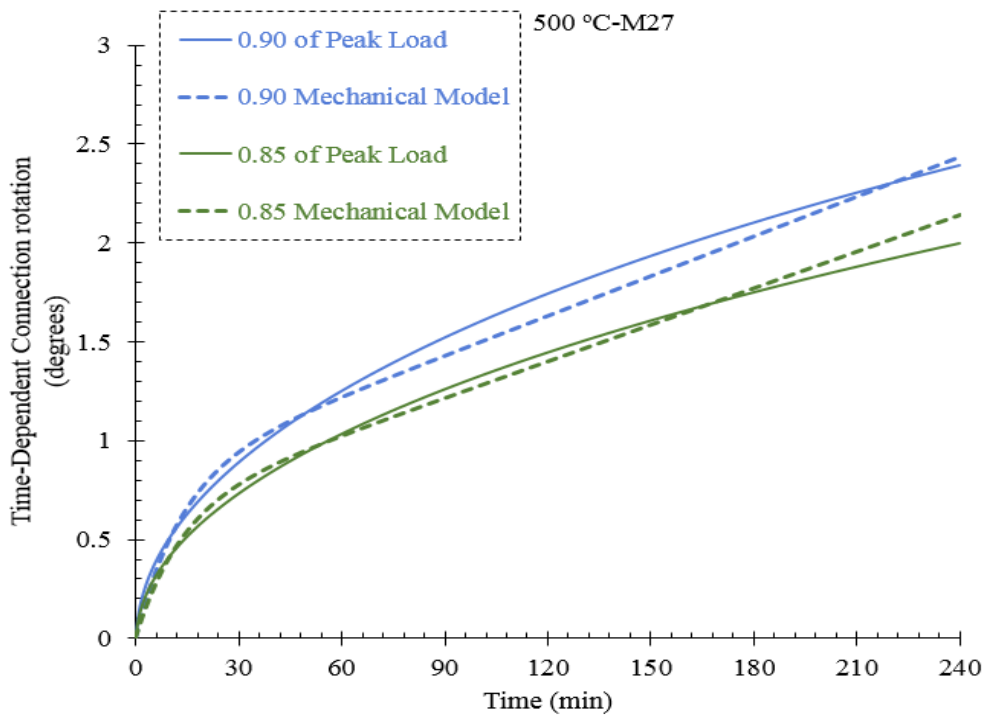
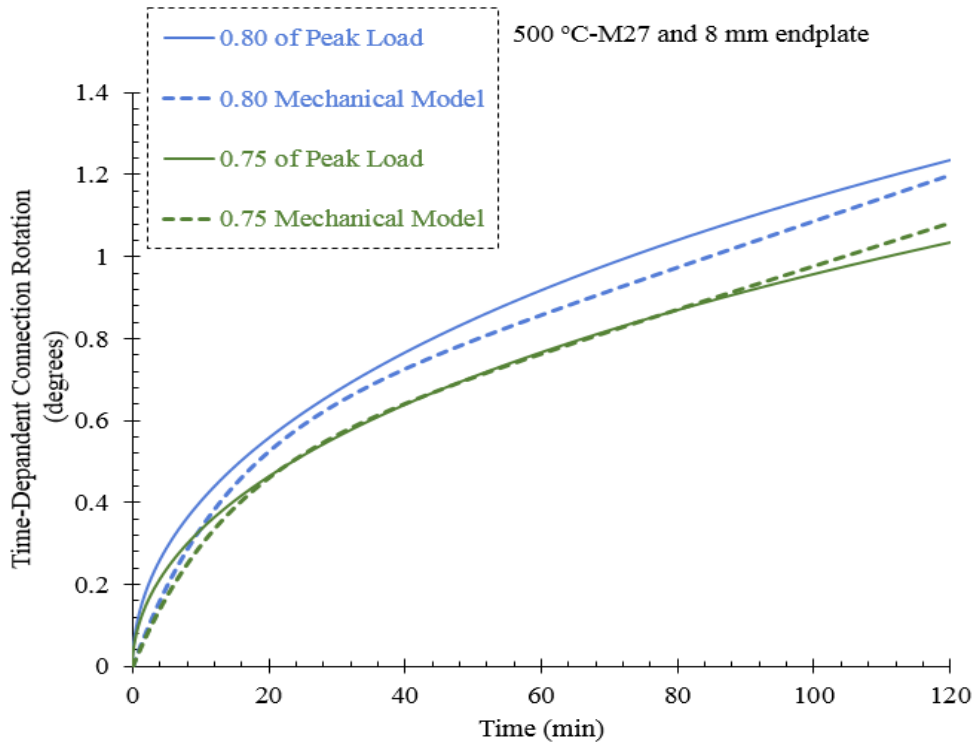


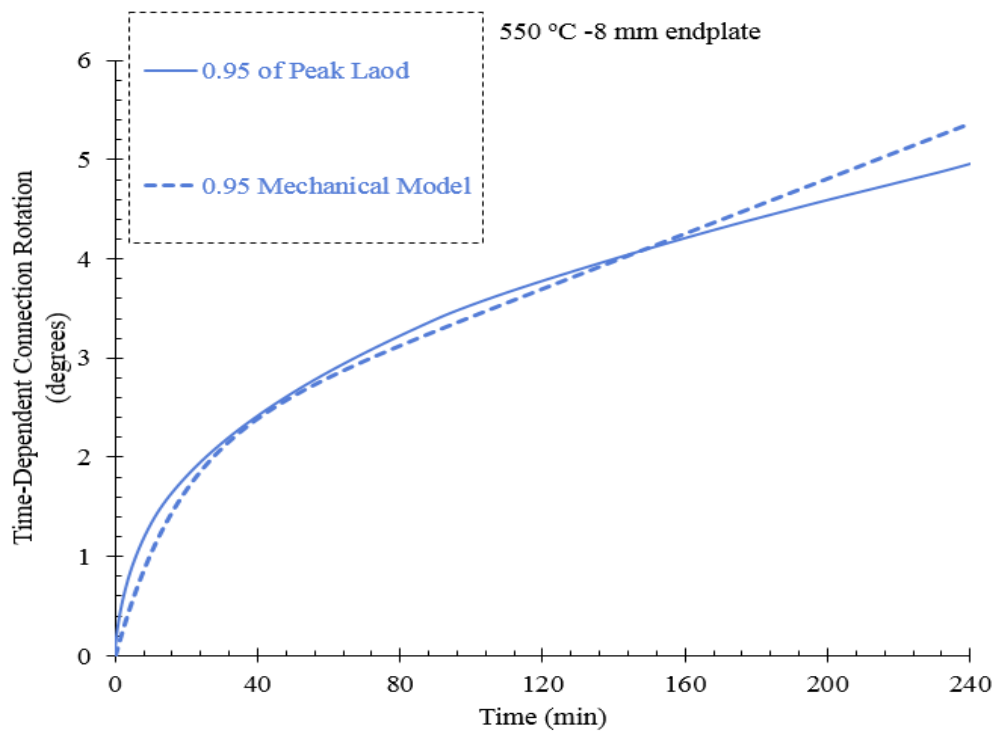
Fig. 31. Isochronous temperature-rotation curves: FE vs. mechanical model time-dependent connection rotation predictions.



(a)



(b)



(c)

Fig. 32. FE vs. mechanical model of flush endplate connection behavior at: (a) 500 °C with M27 bolts, (b) 500 °C with M27 bolts and 8 mm endplate, (c) 550 °C with 8 mm endplate.

CHAPTER VI

SUMMARY, CONCLUSIONS AND, RECOMMENDATIONS

A. Summary and conclusions

Results of FE simulations and mechanical modeling on thermal creep behavior of flush endplate connections in fire were presented. Through a series of FE simulations that were validated against experimental data available in the literature, a methodology was developed to study the time-dependent behavior of flush endplate beam-column connections at elevated temperatures due to fire. Then a proposed mechanical model was developed to predict the force-connection rotation characteristics of flush endplate connections including thermal creep effect. The key conclusions from this research are as follows:

- The proposed mechanical model predict with reasonable accuracy the load-connection rotation response and strength of flush endplate connections at ambient and elevated temperatures when compared to FE simulations and experimental results. The results showed that endplate fracture occurred at low temperatures (20 °C and 450 °C) whereas bolt failure occurred at high temperatures (550 °C and 650 °C) conforming with experimental results available in the literature. In steady-state creep analysis both the FE simulations and the mechanical model show that tension bolt failure governs the connection behavior at temperatures ranging from 450 °C to 600 °C with 25 °C increment. Fracture modeling was not included in the simulation and the FE models were not capable to predict the connection behavior after the first component failure.
- The FE simulations and the mechanical model results showed that the increase in connection rotation due to creep strain can be significant for high temperature, high stress

level, and longer time duration for which building structures are exposed to fire. This emphasizes that ignoring creep may lead to unsafe predictions of structural response of beam-column steel connections when subjected to fire.

- According to the adopted creep model by *Fields and Fields*, the behavior of the selected flush endplate connection is highly time-dependent for temperature above 500 °C.
- Different load angles were incorporated in the analysis. The results show that the variation of load angles does not affect significantly the time-dependent behavior of flush endplate connections when subjected to fire.
- Different plate thicknesses were included in the analysis. The FE simulations show that the slender the endplate is, the larger connection rotation and deformation can be resulted due to creep consideration in the structural steel material properties.
- Larger bolt diameter with different plate thicknesses were included in the analysis. The FE simulations indicate that under steady-state temperature analysis the connection behavior was controlled by endplate failure. As creep was considered in steady-state creep analysis the beam and the endplate tend to relax and connection rotation increases that generates induced tensile stresses in the bolts that leads to tension bolt failure at higher applied loads.
- Based on the results of the FE simulations and the experimental results, a mechanical model was developed to predict the time-independent and time-dependent behavior of flush endplate connections subjected to fire. The results showed that expressions based on the ambient temperature formulations in Eurocode3 where material properties are considered temperature dependent can predict with excellent agreement the time-independent behavior of flush endplate connections in fire. Also, the modified *Burgers* model is capable of

predicting the time-dependent behavior under steady-state and transient-state creep analysis, to define critical times and temperatures for designing steel connections in fire.

- The main advantage of the proposed model is that it requires less computational effort than that required using FE simulations especially when including thermal creep effect. Also, it can be used in more advanced modeling application for structure-fire design.

B. Recommendations

More research work is still needed in order to develop a full understanding of the connection response to fire. This includes:

- A fracture model is needed to be adopted in all FE models which allows a post-yielding analysis of the connection response to fire.
- More work may be conducted to investigate the effect of thermal creep on the behavior on different beam-column connections.
- Additional experimental work on full scale tests, including the thermal creep effect, is needed to be conducted for validation purposes.
- The accuracy of the suggested analyses can be enhanced by including the thermal creep models for structural bolts, and considering the effect of different fire scenarios on the connection response including thermal creep effect.

BIBLIOGRAPHY

- Al-Jabri, K. S., Seibib, A., and Karrech, A. (2008). "Modelling of Unstiffened Flush End-Plate Bolted Connections in Fire," *J. Constr. Steel Res.*, 62, 151-159.
- Yu, H., Burgess, I., Davison, J., and Plank, R. (2011). "Experimental and Numerical Investigations of the Behavior of Flush End Plate Connections at Elevated Temperatures," *J. Struct. Eng.*, 80-87.
- Li, J.-T., Li, G.-Q., Lou, G.B., and Chen, L.-Z. (2012). "Experimental Investigation on Flush End-plate Bolted Composite Connection in Fire," *J. Constr. Steel Res.*, 121-132.
- Gao, Y., Hongxia, H., and Gang, S. (2013). "Resistance of Flush Endplate Connection under Tension and Shear in Fire," *J. Constr. Steel Res.*, 86, 195-205.
- Hantouche, E. G., Abboud, N. H., Morovat, M. A., Enghardt, M.D. (2016). "Analysis of steel bolted angle connections at elevated temperatures" *Fire Safety Journal*, 83, 79-89.
- Hantouche, E. G., and Sleiman, S. A. (2016). "Response of double angle and shear endplate connections at elevated temperatures" *International journal of steel structures*, 16(2), 489-504.
- Loster-Jones, L., "The influence of semi-rigid connection on the performance of steel framed structures in fire", Ph.D dissertation, University of Sheffield, 1997.
- Da Silva, L.S., Santiago, A., Real, P.V. (2001) "A component model for the behavior of steel joints at elevated temperature", *J. Constr. Steel Res.*, 57, 1169-1195.
- Block, F.M., Burgess, I.W., Davison, J.B., Plank, R. J. (2007). "The development of a component-based connection element for endplate connections in fire", *Fire Safety Journal*, 42(6-7), 498-506.

- Huang, Z. (2011). "A connection element for modelling end-plate connection in fire", *J. Constr. Steel Res.*, 67, 841-853.
- Al-Jabri, K.S. (2004). "Component-based model of the behaviour of flexible end-plate connections at elevated temperatures", 66, 215-221.
- Hantouche E.G., Sleiman S.A. (2017). "Axial restraint forces in shear endplates of steel due to fire", *J. Constr. Steel Res.*, 128, 528-541.
- Morovat, M. A., Lee, J., Engelhardt, M. D., Helwig, T. A., and Taleff, E. M. (2011). "Analysis of Creep Buckling of Steel Columns Subjected to Fire," *Structures Congress, ASCE*, 2929-2940.
- Morovat, M. A., Lee, J., Engelhardt, M.D., Taleff, E. M., T. A. Helwig, T. A, and Segrest, V. A. (2012). "Creep Properties of ASTM A992 Steel at Elevated Temperatures", *Advanced Materials Research*, 446-449, 786-792.
- Kodur, V. K. R., and Dwaikat, M. M. S. (2010). "Effect of High Temperature Creep on the Fire Response of Restrained Steel Beams" *Materials and Structures*, 43, 1327-1341.
- Li, G.-Q., and Guo, S.-X. (2008). "Experimental on Restrained Steel Beams Subjected to Heating and Cooling," *J. Constr. Steel Res.*, 64, 268-274.
- Harmathy, T. Z. (1967). "A Comprehensive Creep Model" *J. of Basic Eng., Trans. ASME*, 89(3), 496-502.
- Li, G.-Q., and Zhang, C. (2012). "Creep Effect on Buckling of Axially Restrained Steel Columns in Real Fires," *J. Constr. Steel Res.*, 71, 182-188.
- Lie, T. T., and Macaulay, B. A. 1989. "Evaluation of the fire resistance of protected steel columns," *Internal Report No. 583*, National Research Council Canada.

Fields, B. A., and Fields, R. J. (1989). “Elevated Temperature Deformation of Structural Steel,”
Report NISTIR 88-3899, NIST, Gaithersburg, MD.

El Ghor, A.H., Hantouche, E.G., Morovat, M.A., Engelhardt M.D. (2016). “Creep Behavior of
Flush Endplate Connections at Elevated Temperatures Due to Fire”. *Structures in Fire
Proceeding of the ninth international conference*, Princeton University, New Jersey, USA,
435-442.

Torić, N., and Burgess, I. W. (2016), “A unified rheological model for modelling steel behaviour
in fire conditions”, *J. Constr. Steel Res.*, 127, pp. 221-230

Norton, F.H. (1929). “The Creep of Steel at High Temperatures”. New York: McGraw-Hill
Book Company, Inc.

<http://fire-research.group.shef.ac.uk/downloads.html>, November, 2007.

Lee J., Morovat, M .A., Hu, G., Engelhardt, M. D., and Taleff, E. M. (2013). “Experimental
investigation of mechanical properties of ASTM A992 steel at elevated temperatures,” *Eng.
J.*, 50(4), pp. 249-272.

Hu, Y., Davison, J. B., Burgess, I. W., and Plank, R.J. (2007). “Comparative Study of the
behaviour of BS 4190 and BS EN ISO 4014 bolts in fire,” *Proc., ICSCS*, Taylor & Francis,
London, pp. 587–592.

Findley, W.N., Lai, J.S., and Onaran, k. (1976), “Creep and relaxation of nonlinear viscoelastic
materials” North-Holland Publishing Company-Amsterdam New York-Oxford.